

# How to Get the Best Gas Separation Membranes from State-of-the-Art Glassy Polymers

Nicholas E. León, Zhongyun Liu, Maryam Irani, and William J. Koros\*



Cite This: *Macromolecules* 2022, 55, 1457–1473



Read Online

ACCESS |



Metrics & More

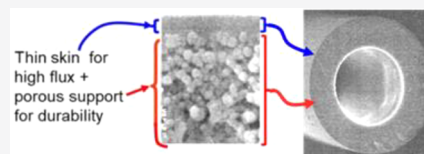


Article Recommendations



Supporting Information

**ABSTRACT:** Herein we focus on fundamental polymer science factors in membrane-based gas separation to open another chapter on this important topic. Realistically thinking about nanometer and angstrom scale matrix attributes that are translatable into higher performance thin glassy polymer asymmetric membrane layers in practical large-scale devices is crucial. Such thinking should be guided by expertise in both polymer and membrane communities to advance the state-of-the-art. Polymer structures, membrane morphologies, and effects of operating conditions are discussed here by using specific examples to illustrate key issues. Rubbery polymers are not the focus of this discussion since they lack diffusive discrimination for size-similar penetrants, which glassy polymers provide and make them the focus here. Four scalable subtopics guide necessary thinking: (i) plasticization, (ii) antiplasticization, (iii) dual-mode transport involving saturation of unrelaxed free volume, and (iv) nonuniform free volume and stress profiles in thin skin glassy polymer asymmetric or composite membranes. Using these subtopics in the context of macromolecular science, we discuss issues needed to expand the state-of-the-art in gas separation membranes.



## INTRODUCTION

The domain in Figure 1 of A/B selectivity,  $\alpha_{A/B}$  (eq 2), vs permeability of A,  $P_A$  (eq 1), with a dashed trade-off line for

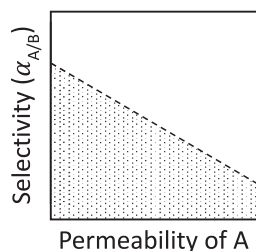


**Figure 1.** Domain of solution-processable polymers (shaded region) from which gas separation membrane candidate polymers are selected for a given A/B pair.

solution-processable polymers helps identify top candidates for gas separation membranes for a given A/B penetrant pair.<sup>1–4</sup> Sorption selectivity is controlled by A/B critical temperature and their interactions with the membrane material, while diffusion selectivity is controlled by A/B size and polymer structure. While useful, such trade-off plots, for a particular A/B pair, overlook additional crucial issues involved in delivering the best possible gas separation membranes. Specifically

$$P_i = S_i D_i \quad (1)$$

$$\alpha_{A/B} = \frac{P_A}{P_B} = \frac{S_A D_A}{S_B D_B} \quad (2)$$

understanding four additional factors—(i) plasticization,<sup>5</sup> (ii) antiplasticization,<sup>6</sup> (iii) dual-mode transport involving saturation

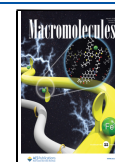
of unrelaxed free volume,<sup>7</sup> and (iv) nonuniform free volume and stress profiles in thin skin glassy polymer layers of asymmetric or composite membranes<sup>8</sup>—is also crucial. Indeed, such factors can be as important to success as is a polymer's location on permeability–selectivity trade-off plots like Figure 1.

To enable focus, Figure 2a (flexible) and Figure 2b (semirigid) glassy polymers with some segmental motions are considered here based on their broad potential as next-generation polymer membranes.<sup>9</sup> Rigid microporous materials (Figure 2c), which lack framework motions, will only be discussed briefly for cases wherein Figure 2a,b materials are inadequate. “Zones of activation” shown in green in Figure 2a,b arise from local segmental motions and can increase (plasticization) or decrease (antiplasticization) due to sorbed penetrants and affect diffusion strongly. Plasticization (item i),<sup>5</sup> the best known of the four factors, leads to increased diffusion coefficients and may reduce diffusion selectivity based on size if zones of activation increase excessively. As discussed later, in some cases, moderate controlled plasticization may be useful to offset productivity losses while maintaining attractive selectivities, which we believe is a broad and general feature. Because of currently limited data, this principle is discussed for a polymer below the CO<sub>2</sub>/N<sub>2</sub> upper bound; however, the generality of the principle for many A/B pairs makes this approach worthwhile.

**Received:** August 19, 2021

**Revised:** February 11, 2022

**Published:** February 24, 2022



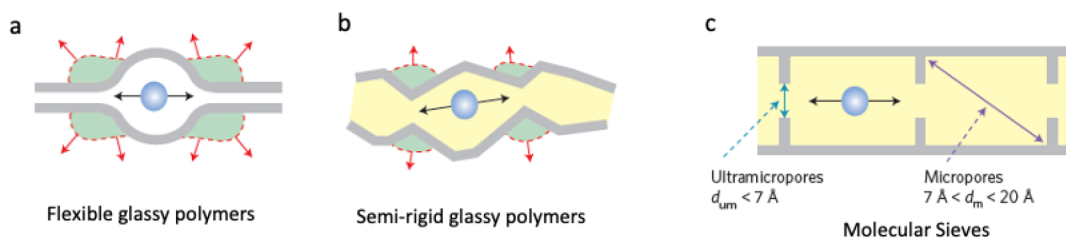


**Figure 2.** Molecular diffusion selective media. (a) Flexible polymers with transient gap distributions created by segmental packing and motion. (b) Semirigid polymers with connected porosity distributions created primarily by segmental packing. (c) Molecular sieves with rigid ultramicropore and micropore morphologies. In the case of semirigid polymers (b) and molecular sieves (c), the yellow shaded areas represent permanent connected porosity which is not present in flexible polymers (a). The green shaded areas represent motion-enabled zones of activation needed for diffusion. Reproduced with permission from ref 9. Copyright 2017 Springer Nature.

Item ii, antiplasticization,<sup>6,a</sup> arises when low ppm levels of copermeating contaminants such as toluene are present in an otherwise simple binary gas feed and can hinder polymer segmental motions and reduce the zone of activation. At higher levels of such copermeating components, transition can occur from antiplasticization to plasticization (item i).<sup>5</sup> Item iii involves “dual mode” effects due to competition of copermeating components for semipermanent nonequilibrium packing disruptions in glassy polymers illustrated in Figure 3.<sup>7,10</sup> Such long-lived free volume packets are idealized as “unrelaxed volume” within nonequilibrium glassy polymers illustrated.

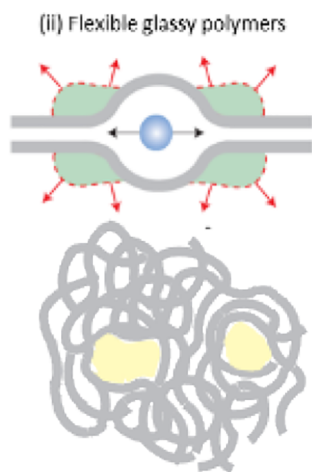


**Figure 3.** Low volume percent  $<5 \text{ \AA}$  segmental packing distribution Langmuir phase (yellow) in continuous amorphous segmental phase gray segments.

The term “dual mode” refers to such coexisting unrelaxed segmental packing features within a majority equilibrium glassy matrix. Effects of such features are conveniently described by so-called dual-mode sorption and transport models that help understand trends for glassy films with pure and mixed gases.<sup>7,9</sup> The selective skin layer is the most crucial feature<sup>9</sup> (Figure 4), and a description of properties of this layer is also possible in terms of the dual mode framework. The fourth attribute (iv), nonuniform free volume and stress profiles that arise during rapid phase inversion (quenching) or thin film composite casting, is also partially understandable within the dual mode framework.<sup>8</sup> Studies focused only on dense films overlook this feature (Figure 4b), which differs from the overall asymmetric membrane morphology comprising skin, transition, and support layers (Figure 4a). The term “vectored” is used here for factor iv to refer to unrelaxed free volume and stress profiles in the

selective layer (i.e., skin). Figure 4b illustrates unrelaxed free volume in the skin. Such features can be generated in typical asymmetric membrane spinning processes<sup>8,11</sup> (see Figure S-1). Clausi<sup>8</sup> illustrated effects of vectoring by studies in Matrimid (Figure 5) asymmetric hollow fibers using pure component  $\text{CO}_2$ ,  $\text{CH}_4$ ,  $\text{O}_2$ , and  $\text{N}_2$  feeds at only 50 psia to avoid plasticization complications that might obscure the effect. These four gas probes are useful, since  $\text{CH}_4$ ,  $\text{O}_2$ , and  $\text{N}_2$  show minor dual mode effects in glassy polymers, while the more condensable  $\text{CO}_2$  shows strong dual mode effects.<sup>12</sup> A 34% higher  $\text{CO}_2$  permeance difference was observed for bore vs shell feed, while a negligible 2% higher  $\text{O}_2$  permeance difference for bore vs shell side feeds was seen.<sup>8</sup> Such results reflect a higher unrelaxed volume profile from bore to shell side of the defect free skin, reflected as a higher unrelaxed Langmuir capacity factor,  $C_{H'}$ , near the bore side of the skin. The more condensable  $\text{CO}_2$  vs  $\text{O}_2$  benefits most from bore side vs shell side feed mode.

Clearly, (i) plasticization, (ii) antiplasticization; (iii) dual mode effects, and (iv) vectoring effects are connected to traditional features such as polymer molecular weight, glass transition temperature, and fractional free volume known to our polymer community. These aforementioned items along with Figure 1 comprise an effective set of tools to produce the best possible gas separation membranes. Polymer types a and b in Figure 2 and all families in Figure 6 can deliver advanced membranes by using the strategy here. Emerging materials may join this group, but these 3 broad families are currently the most likely to deliver high permeability and adequate selectivity in the near term. Studying asymmetric membranes and thin film composites for a candidate polymer, even if only in flat sheet forms under relevant feed conditions will avoid unpleasant application surprises for a given gas pair.

External mass transfer resistances for gas separations can be managed,<sup>13</sup> but for high-permeability materials with ( $<1 \mu\text{m}$ ) selective layers, approximate guidelines should be kept in mind. For example, a membrane with high  $\text{CO}_2$  permeability (842 barrer)<sup>14</sup> and  $1 \mu\text{m}$  micrometer skin in low-pressure flue gas feeds with 12–13 psi  $\text{CO}_2$  partial pressure feed driving forces avoids such problems. Nevertheless, the same polymer with 50–60%  $\text{CO}_2$  feed at 30 atm could encounter “concentration polarization” due to high flux, creating external resistance in series with the intrinsic selective layer to reduce both selectivity and productivity. Tangential flow at the surface can avoid problems in this situation. This fact notwithstanding a “highly advanced” material with still higher 1600 barrer permeability and  $1 \mu\text{m}$  skin for a 60 atm feed would require additional module design elements to manage, while beyond the scope of this discussion it is useful to keep this topic in mind.<sup>13</sup> Also, so-called

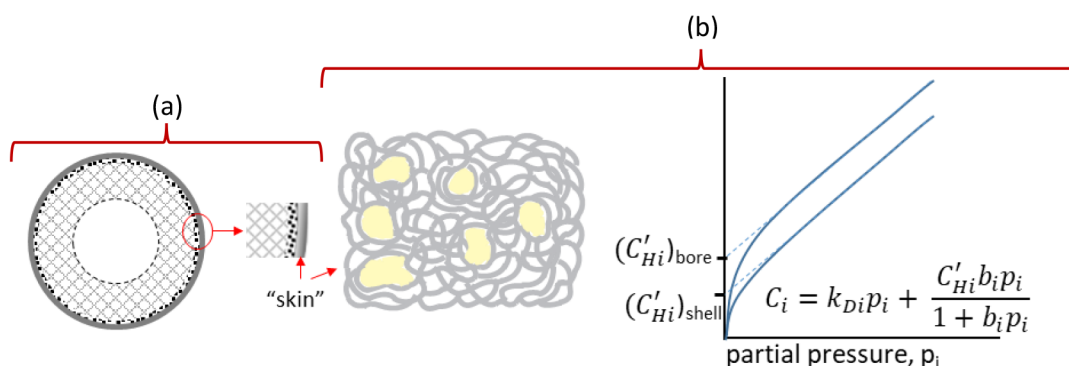


**Figure 4.** (a) Schematic of an idealized asymmetric hollow fiber with inner porous support, transition layer, and outer idealized “vectored skin”. (b) Idealized unrelaxed volume “vectored skin” with higher unrelaxed volume profile, causing higher  $C_{H'}$  near transition layer (bore side) vs outer (shell side) of skin.

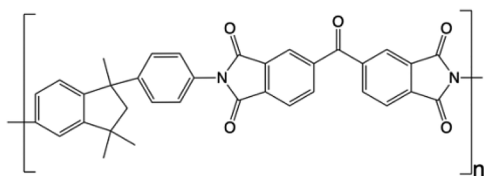


**Figure 5.** Chemical structure of Matrimid 5218.

“frame of reference effects”<sup>15</sup> encountered in high-flux membranes can undermine diffusion selectivity. Fortunately, fiber modules package roughly 10×–100× more membrane area per volume than other module forms, thereby avoiding the need for superhigh fluxes. This advantage delivers high module productivity and indirectly overcomes both above practical problems. We feel this fact suggests that hollow fibers with high, not superhigh, intrinsic permeability materials with thin selective skin thicknesses on hollow fibers are most appealing for advanced membranes.

We also focus on asymmetric structures because thin glassy structures can behave as “amplifiers” for tendencies for (i) plasticization, (ii) antiplasticization, (ii) dual mode, and (iv) vectoring effects—especially for high free volume materials. If a polymer candidate shows different attributes i–iv in asymmetric vs dense membrane formats, this is an “alert” to understand the effects as early as possible, as illustrated with examples below. Fortunately, macromolecular fundamentals lie at the basis of such issues, making this topic ideal for this discussion. The polyimide (PI) family in Figure 6, typical of flexible glassy polymers in Figure 2a, has been explored most completely in the context of the above-recommended approach with asymmetric structures.<sup>16–22</sup> Following a similar approach for thermally rearranged (TR)<sup>23–25</sup> and polymers of intrinsic microporosity (PIM)<sup>25–31</sup> families, typical of semirigid polymers in Figure 2b, would be wise. While these latter two families offer appealing selectivity and resistance to plasticization, they can show strong

susceptibility to (ii) antiplasticization, (iii) dual mode competition, and (iv) vectoring factors. Members of these families must be evaluated in terms of such factors—preferably in asymmetric or thin film composite formats to clarify the extent of “amplifying features” noted above to be more than academic curiosities. We use the PI family as an exemplar of all families in Figure 6, but a discussion of polyimides should stimulate similar work for the TR and PIM families (and others) by our community.

Physical aging of glassy polymers is a general topic of interest to polymer scientists,<sup>32,33</sup> and the membrane area is cognizant of the topic. In fact, the topic appears to have first received attention in membranes for thin film polymer–ceramic composite membranes close to 30 years ago.<sup>34</sup> In that case, a high- $T_g$  polyimide and polycarbonate with layers in the range of 0.4  $\mu\text{m}$  showed dramatic aging when cast on ceramic supports. Since that time, extensive work with various sophisticated techniques and analyses<sup>35–39</sup> ultimately identified diffusion of free volume and lattice contraction as key fundamental factors responsible for the effects. Especially for the high fractional free volume TR and PIM families, aging-induced permeability reductions and selectivity increases for various gas pairs<sup>36,40–42</sup> have been reported. Fortunately, such effects tend to be less important for asymmetric membranes with equivalent selective layers (Figure 4) due to their formation protocols (Figure S-1). Specifically, unlike cast thin film composites, asymmetrics usually undergo postspinning water soaking to remove residual solvents, followed by solvent exchange with methanol and then hexane solvent exchange to avoid transition layer and support layer collapse (Figure S-1). These steps mitigate stress artifacts but leave unrelaxed volume profiles illustrated in Figure 4 unless followed by postdrying annealing. The aging topic will be revisited later after addressing (i) plasticization, (ii) antiplasticization, (ii) dual mode, and (iv) vectoring effects.

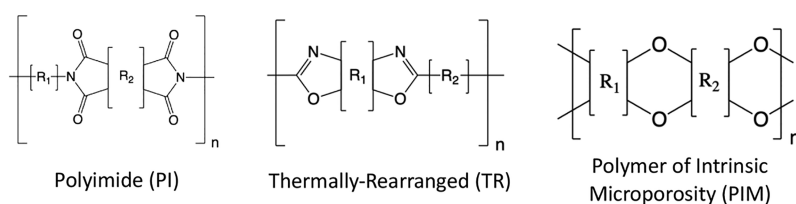


**Figure 6.** Three important families of glassy polymers that have potential to advance the state of the art in membrane-based gas separations.

Pioneering work by Hoehn and co-workers<sup>43–45</sup> opened a new chapter in the gas separation story using polyimide membranes. The 6FDA-6FpDA polyimide (Figure 7) was

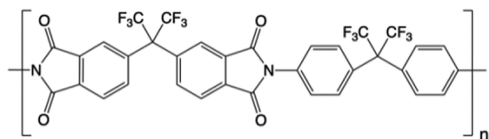


Figure 7. Chemical structure of 6FDA-6FAP.

identified as a material to move beyond first-generation commercial engineering polymers. Later work<sup>46</sup> showed negligible plasticization (dense film samples with molecular weight  $\sim 3 \times 10^5 M_w$ ) up to 10 atm. Mikawa et al.<sup>47</sup> further studied  $\text{CO}_2$  plasticization resistance of this polyimide in actual asymmetric formats. This study reported gas permeances of pure  $\text{CO}_2$ ,  $\text{N}_2$ ,  $\text{O}_2$ , and  $\text{CH}_4$  for defect-free asymmetric membranes at 35 °C for feed pressures up to 10 atm with vacuum permeate conditions. Consistent with the dense film study, plasticization was not observed for a high-molecular-weight polyimide sample ( $4.3 \times 10^5 M_w$ ) in asymmetric hollow fibers.<sup>47</sup> Surprisingly, however, fibers created by using a lower-molecular-weight ( $1.2 \times 10^5 M_w$ ) sample showed  $\text{CO}_2$  plasticization starting at quite low feed pressure ( $\sim 2.6$  atm). If traditional free volume contributed by chain ends were the dominant issue, such plasticization at low pressures would make this result surprising, given the already sparse chain ends in the  $1.2 \times 10^5 M_w$  sample. This case is an example of an “alert” to understand a surprising effect. Recent state-of-the-art molecular simulation work on sorption and plasticization of 6FDA-FpDA, including for mixed gases, is pertinent here.<sup>48</sup> This simulation study detected item iii (dual mode type sorption responses) due to more sorptive  $\text{CO}_2$  competitively reducing the sorption of both  $\text{CH}_4$  and  $\text{N}_2$  in the glassy unrelaxed volume. Also, consistent with the dense film results of Coleman,<sup>46</sup> the simulation showed that the  $\text{CO}_2$  concentration was below the point at which plasticization of the polymer was expected. The surprising plasticization sensitivity detected by Mikawa therefore may reflect molecular-weight effects suggesting item iv (skin vectoring in Figure 4) arising during asymmetric membrane formation rather than a traditional bulk property per se. The above combined results highlight the more complex nature of glassy polymer vs rubbery polymer membranes and show synergies between advanced simulation, dense film and asymmetric fiber studies as a model for future materials. Indeed, this example shows that dense film studies are an important but incomplete first step toward realistic advanced membrane development for all new material families.

Following the above theme, related work on 6FDA polyimides based on ODA, MDA, IPDA, and DAF<sup>49</sup> diamines showed strong dual mode sorption behavior with little or no

plasticization up to 10 atm of pure  $\text{CO}_2$ . Matsumoto considered the 6FDA-ODA polyimide<sup>50</sup> (Figure 8b) and extended the prior work by Kim to considering not only dense film properties but also asymmetric membrane properties. As with the 6FDA-6FpDA material, evidence of typical dual mode permeability vs pressure behavior (factor iii) was seen in both the dense film and asymmetric membrane cases. Moreover, a lack of plasticization effects was reported up to 10 atm; however, plasticization became apparent above 10 atm. Matsumoto also took another key step by studying the rigid diamine *p*-phenylenediamine (pPDA) and found the absence of plasticization up to 10 atm in both dense film and asymmetric membrane samples. This study revealed that the rigid diamine pPDA not only gave higher  $\text{CO}_2/\text{CH}_4$  selectivity but also higher  $\text{CO}_2$  permeability and asymmetric membrane permeance ( $P/L$ ) vs the material with the flexible backbone ODA structure. Moreover, evidence was reported for extra free volume in the thin skin, suggesting possible “vectoring” based on combined analysis of SEM and dense film permeation properties.

Later, Hayes at DuPont took an important step beyond the pPDA diamine and used diaminomesitylene (DAM) and durene diamines as single-ring aromatic diamines.<sup>51</sup> Also, the idea of photo-cross-linking was explored. Most importantly, even without photo-cross-linking, by addition of the bulky  $\text{CH}_3$  groups, packing inhibition and rotational motion inhibition were achieved simultaneously, which led to dramatic permeability increases, at some cost to selectivity. The so-called DAM diamine (with three  $\text{CH}_3$ 's) and durene diamine (with four  $\text{CH}_3$ 's) produced a huge  $20\times$ – $30\times$  permeability increase due to more packing inhibition and with roughly a  $2\times$  reduction in  $\text{CO}_2/\text{CH}_4$  selectivity prior to the onset of plasticization. It soon became clear that the above tools could allow balancing productivity and selectivity in more advanced materials for gas pairs even beyond  $\text{CO}_2/\text{CH}_4$ . Plasticization onset was extended from around 10 atm  $\text{CO}_2$  partial pressure to around 20 atm by copolymerization with BPDA (see Figure 9), a less packing-inhibiting dianhydride, to regain attractive selectivities in high performance asymmetric fibers.<sup>51–54</sup>

As increasingly aggressive feeds were faced, item ii (anti-plasticization) was encountered in glassy polymer membranes. In dense glassy polycarbonate in 1983<sup>55</sup> significant permeability depression was noted and attributed simply to dual mode competition for “Langmuir” excess unrelaxed volume in Figure 3. In hindsight, antiplasticization, leading to depression of diffusion within the non-Langmuir glassy equilibrium matrix, was probably also at play; however, it was not realized initially. Later surprises in actual field operations wherein aromatic C6–C8 contaminants caused generalized depression of permeability coefficients throughout the glassy matrix due to true antiplasticization were identified. This discovery showed antiplasticization and dual mode effects had to be dealt with. Once understood, controlling antiplasticization by using sorbent guard beds to reduce partial pressures of such contaminants

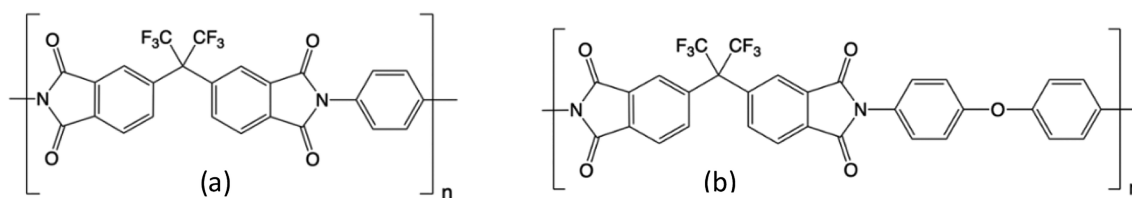
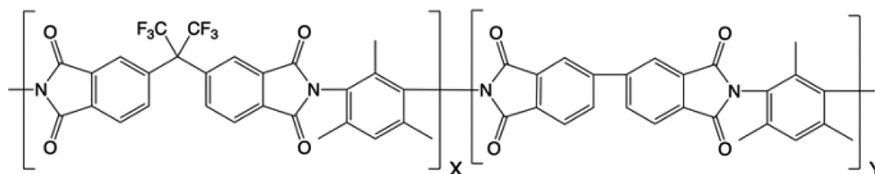
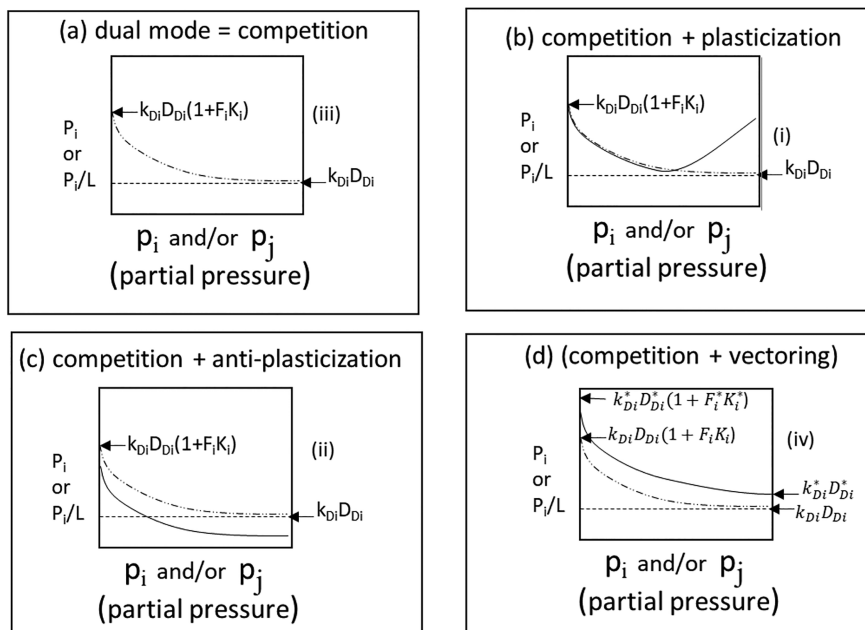


Figure 8. Chemical structures of (a) 6FDA-pPDA and (b) 6FDA-4,4'-ODA.



**Figure 9.** Chemical structure of the 6FDA:BPDA-DAM copolymer. The ratio of X:Y is 1:1.



**Figure 10.** Schematic representations of (a) dual mode competition, (b) dual mode competition and plasticization, (c) dual mode competition and antiplasticization, and (d) dual mode plasticization and vectoring as solid lines. As noted earlier, the double-dot-dashed lines (·····) from eq 3 response with only dual mode competition effects. Combination of attributes are of course possible. For asymmetric case,  $P_i$  and  $k_{D_i}D_{D_i}$  are simple replaced by  $P_i/L$  and  $k_{D_i}D_{D_i}/L$ , where  $L$  is the effective selective layer thickness.

became accepted practice in well-designed membrane units. While tuned antiplasticization might offer ways to stabilize against plasticization by tuning pretreatment levels of heavier components, avoiding trace condensable C5–C8 organics with simple guard beds appears to be currently preferred.

Related to the above topic of antiplasticization, work has been done to show that intentional addition of low-volatility components can be used to tune selectivity and permeability.<sup>56</sup> While workable, this appears to have been eclipsed by more conventional structure–property tuning of polymer backbones that eliminate concern about long-term losses of the antiplasticizer. Reliable covalent approaches to address plasticization can be integrated into fiber formation process by judicious selection of polymer structure and processing, without adding excessive costs, as discussed below. A recent noncovalent cross-linking using strong hydrogen bonding between polymer chains and additives has been discussed.<sup>57</sup> Such hydrogen-bonding agents, however, may have antiplasticization effects to reduce productivity and be less stable under aggressive feeds that could extract the hydrogen-bonding agents when extended to actual asymmetric membranes.

## ■ TRANSPORT AS A SENSITIVE ANALYTICAL TOOL

In the absence of plasticization or antiplasticization, the dual mode transport model<sup>12</sup> (eq 3) gives reasonable performance predictions for conventional dense films by using only pure

component sorption and diffusion parameters, viz.,  $k_{D,i}$ ,  $C'_{H,i}$ ,  $b_i$  (with  $K_i = \frac{C'_{H,i}b_i}{k_{D,i}}$ ),  $D_{D,i}$ ,  $D_{H,i}$  (with  $F_i = \frac{D_{H,i}}{D_{D,i}}$ ) in eq 3.

$$P_i = k_{D,i}D_{D,i} \left[ 1 + \frac{F_i K_i p_{i2} / (p_{i2} - p_{i1})}{1 + b_A p_{A2} + b_B p_{B2} + b_C p_{C2}} - \frac{F_i K_i p_{i1} / (p_{i2} - p_{i1})}{1 + b_A p_{A1} + b_B p_{B1} + b_C p_{C1}} \right] \quad (3)$$

$$\alpha_{ij} = \frac{P_i}{P_j} \quad (4)$$

Deviations from model predictions for the simplest case involving a pure component and a downstream vacuum permeate at a given feed component pressure (or partial pressure) give insights into (i) plasticization, (ii) antiplasticization, (iii) dual mode, and (iv) vectoring effects. Permeabilities for a component (i.e., A, B, or contaminant, C) are given by eq 3 for conditions set by upstream and downstream mixture partial pressures  $p_{i2}$  and  $p_{i1}$ , respectively (in Figure 10). Asymmetric membrane case trends for the above equations simply require using  $P_i/L$  (permeance) and  $D_{D,i}/L$ , where  $L$  is the effective skin thickness. The decrease in  $P_i$  or  $P_i/L$  with increasing feed pressures for the case of a vacuum permeate is shown in Figure 10a, reflecting simple competition for Langmuir capacity unrelaxed free volume. This “base case”, shown as a double-

dot-dashed line, helps identify existence of items i–iv, even without detailed fitting of dual mode parameters by simply matching the observed data trend in a given situation to the “fingerprint responses” in Figure 10. The sample dashed lines correspond to  $k_D, D_D$ , the ideal asymptote of eq 3 at high pressure. Similar general trends apply for a 1 atm or other nonvacuum permeate cases based on eq 3, so such plots are simple but valuable tools. While long-lived Langmuir free volume and conventional intersegmental free volume coexist in glassy polymers, changes in the latter intersegmental free volume are expected to be primarily reflected by conventional plasticization (or antiplasticization). When plasticization or antiplasticization is present, the Figure 10(b or c) fingerprints apply.

Studies with TR and PIM materials suggest the dual mode eq 3 applies<sup>23–31,58–61</sup> reasonably, and in such cases, trends noted in Figure 10 can still be “fingerprints” to detect the dominant i–iv attributes for these families in dense film and asymmetric formats. Even without fiber spinning, characterization of flat sheet asymmetric membranes or simple thin film cast composites can avoid surprises as selective layer thicknesses are reduced for all the families in Figure 6. For instance, identifying the molecular weight sensitivity to plasticization in asymmetric formats detected by Mikawa et al.<sup>47</sup> for the 6FDA-6FpDA polyimide mentioned above allowed simple mitigation using higher-molecular-weight samples.

## GLASSY POLYMERS FOR AGGRESSIVE COMPLEX FEEDS

Natural gas comprises a hugely important area with a diverse array of feeds in terms of compositions and available pressures to drive the separation; however, many are very aggressive to membrane materials. For CO<sub>2</sub>/CH<sub>4</sub> binaries, CO<sub>2</sub>/CH<sub>4</sub>/H<sub>2</sub>S ternaries, and CO<sub>2</sub>/CH<sub>4</sub>/H<sub>2</sub>S/hydrocarbon contaminant cases, the dual mode model still provides a quantitative framework to discuss the complex issues involved in such systems. Spectroscopy and molecular simulation help connect polymer structure to factors i–iv; however, asymmetric formats and thin composite membranes tested with mixed gas feeds remain very simple economical “bottom line” analytical tools. The creativity of polymer chemists and ability to produce many structures may make it surprising that new polymers are slow to be adopted in practice. In large measure, one can say “the devil is in factors i–iv”. The earlier mentioned example of antiplasticization is an object lesson regarding the importance of finding problems and solutions in the lab rather than in the field. Large-scale systems are costly, and problems are remembered for many years. Of course, innovation involves risk, but adequate testing of attractive “new candidate polymers” in terms of items i–iv provides a relatively safe path for innovation—even for aggressive feeds.

The common definition of “defect free” in the gas separation membrane community is taken to mean an actual membrane shows a selectivity for a chosen gas pair  $\geq 90\%$  of the polymer’s dense film value. This standard will be used throughout this section, and asymmetric polyimide fibers to be discussed meet this standard, thereby allowing trends to be related to fundamental properties of the selective skin layers. First, we consider feeds with stronger plasticization (item i) tendencies compared to the CO<sub>2</sub>/N<sub>2</sub> case by focusing on CO<sub>2</sub>/CH<sub>4</sub> binaries, followed by addition of an antiplasticizing toluene contaminant (item ii). We next consider “sour” gas mixtures (CO<sub>2</sub>/H<sub>2</sub>S/CH<sub>4</sub>) and CO<sub>2</sub>/H<sub>2</sub>S/CH<sub>4</sub> with contaminants to

illustrate effects of attributes i–iv for advanced materials in asymmetric formats.

As a first step to understand aggressive feeds and their key issues, insights from a few important prior studies are useful. Visser et al.<sup>62</sup> considered plasticization effects in advanced blend composite asymmetric hollow fibers based on Matrimid and poly(ether sulfone) for both CO<sub>2</sub>/N<sub>2</sub> and CO<sub>2</sub>/CH<sub>4</sub> gas binaries. The pressure dependence on the gas permeance was determined over the range from 4 to 20 bar feed pressure. Vacuum downstream permeate conditions were used, and pure component CO<sub>2</sub>/N<sub>2</sub> and CO<sub>2</sub>/CH<sub>4</sub> permeance ( $P/L$ ) ratios increased as feed pressure increased, reflecting plasticization. Gas mixtures (CO<sub>2</sub> in N<sub>2</sub> or CO<sub>2</sub> in CH<sub>4</sub>) were also studied, and separation factors decreased with increasing mixed gas feed pressure. If only plasticization effects were controlling, the author correctly noted that a steeper reduction in selectivity would be expected at higher CO<sub>2</sub> concentrations in the feed. The lack of such a steep fall was noted as an indication of a subtle balance between item i (plasticization) as well as competitive dual mode effects (item iii). In this case dual mode sorption competition between CO<sub>2</sub> and either CH<sub>4</sub> or N<sub>2</sub> moderates plasticization by reducing the sorbed concentration of CO<sub>2</sub> for either high N<sub>2</sub> or CH<sub>4</sub> feed mixed gas fractions. An additional commercially available material, BTDA-TDI/MDI copolyimide (P84), blended with Matrimid helped suppress plasticization for CO<sub>2</sub>/CH<sub>4</sub> in dense film form.<sup>63</sup> A logical extension to actual asymmetric format for P84) was done—and gave a surprise.<sup>64</sup> Specifically, although stable in dense films for 55:45 CO<sub>2</sub>:CH<sub>4</sub> feeds at 50 bar, upon testing in asymmetric form, P84 plasticization was apparent at even 8 atm of pure CO<sub>2</sub>; moreover, permeances ( $P/L$ ) were low, even after plasticization. This study avoided encountering a surprise in later full scale testing—stressing the importance of asymmetric sample studies.

Awareness of opportunities beyond commercial polymers spurred academic studies of custom-made materials for CO<sub>2</sub>/CH<sub>4</sub> separation, and we focus here on such specialty polymers wherein actual asymmetric formats with mixed gases are considered. As with earlier studies using commercial polymers noted above, starting with dense films and culminating in asymmetric fibers with actual mixtures under aggressive feeds avoided surprises in ultimate scaleup. Work by Chung and co-workers<sup>65,66</sup> used 6FDA-2, 6DAT (Figure 11) as an alternative

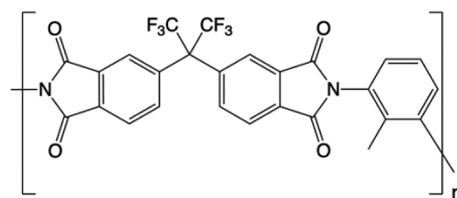


Figure 11. Chemical structure of 6FDA-2,6-DAT.

to the above-mentioned DAM diamine. The initial asymmetric 6FDA-2, 6DAT hollow fiber membranes showed plasticization for both CO<sub>2</sub> and CH<sub>4</sub> even under only a mildly aggressive feed of 40% CO<sub>2</sub>/60% CH<sub>4</sub> up to 200 psia.<sup>65</sup>

The mixed gas permeation used 1 atm permeate pressure. Sub- $T_g$  heat treatment of the hollow fiber membranes at 250 °C (vs  $T_g = 335$  °C) effectively suppressed CO<sub>2</sub>-induced plasticization up to 200 psia CO<sub>2</sub> pure or partial pressure without rendering the fiber insoluble. The heat treatment caused

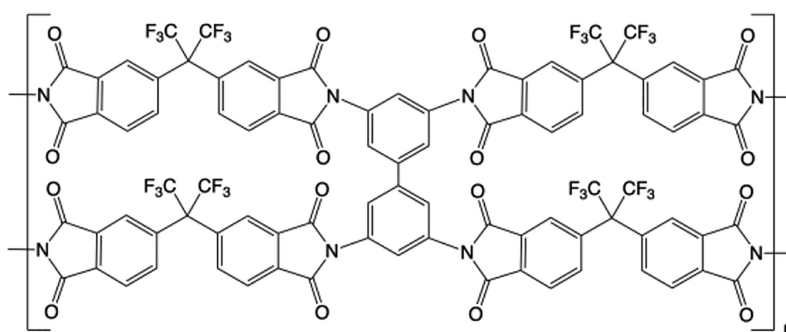


Figure 12. Possible cross-linking sites through the DABA diamines in the free acid 6FDA-DAM:DABA polymer.

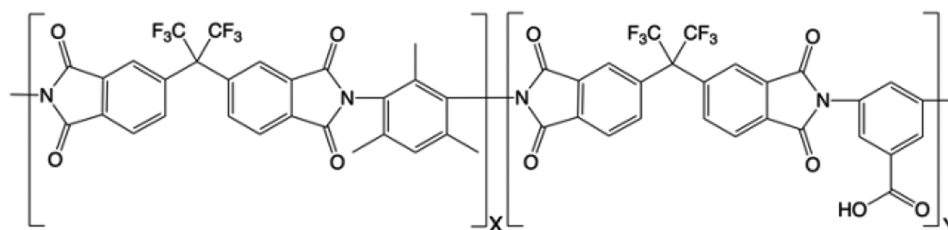


Figure 13. Chemical structure of 6FDA-DAM:DABA. The ratio of X:Y is 3:2.

roughly  $2\times$  reduction in permeance ( $P/L$ ) due to physical densification of both the high free volume outer skin layer and some transition layer (Figure 4a), leading to a thicker effective skin.<sup>67</sup>

Beyond thermally driven densification stabilization, actual chemical cross-linking involving cross-linking with a diamine post-treatment to open some backbone imide rings and bridge between neighboring segments was demonstrated in dense films and also in asymmetric fibers.<sup>51,66</sup> While viable for totally anhydrous feeds, long-term stability of such structures can be compromised by hydrolysis of amic acids, thereby complicating its generality. More general chemical stabilization approaches using groups intrinsically connected to the polymer backbone are appealing to integrate processing into postspinning drying steps (Figure S-1). A recent example explored in dense films used a copolymer of 3,3-bis[4-(4-amino-3-methylphenoxy)phenyl]phthalide (MPP)<sup>68</sup> with 6FDA to increase chain rigidity and allow thermal oxidative cross-linking at relatively low temperatures of only 275 °C. Evidence of factor iii (dual mode penetrant competition) was noted with 50:50 CO<sub>2</sub>:CH<sub>4</sub> mixed gases up to 30 atm. This approach should be translatable to asymmetric formats; however, it has not yet been done. A different approach involving a reactive pendant carboxylic acid group in copolymers of 6FDA-DAM:DABA with tailored DAM:DABA ratios has, however, been shown viable for thermally induced cross-linking in both dense films and asymmetric fibers (Figure 12).<sup>69,70</sup> Sub- $T_g$  cross-linking at 350 °C for a 6FDA-DAM:DABA 3:2 sample shown in Figure 13 (387 °C  $T_g$ ) enabled cross-linking chemistry without support layer collapse. The resultant functional asymmetric membrane maintains its essential polyimide structure, differing from the native polyamide only at cross-link points. The cross-link is attributed primarily to the structure in Figure 12. This approach differs significantly from so-called TR polymers in Figure 6, where actual general backbone rearrangement to the totally different polybenzoxazole linkage occurs typically at above 400–450 °C. Sub- $T_g$  cross-linking as an extension of the postspinning drying step is straightforward with remarkable stability up to

1000 psia feed pressures for 50:50 CO<sub>2</sub>:CH<sub>4</sub> and even 70:30 CO<sub>2</sub>:CH<sub>4</sub> feeds at 35 °C.<sup>71</sup> Because hollow fibers offer roughly  $10\times$  higher surface to volume vs spiral formats, the CO<sub>2</sub> permeances of 40 GPU at 1000 psia and CO<sub>2</sub>/CH<sub>4</sub> selectivities from 35 at 200 psia and 28 at 1000 psia are viable. Approximate SEM estimates of the stabilized skin suggest increases from 0.4 to 4  $\mu\text{m}$  by using treatments from 300 to 350 °C, which suggest opportunities for higher permeances for the 300 °C case by minimizing selective layer thickening. Moreover, mild plasticization associated with lower cross-linking at 300 °C also maintains thinner skins, while possibly giving double benefits by also offsetting dual mode (item iii) induced permeance declines. Finally, during essentially all annealing for cross-linking, stresses and excess volume trapped during spinning can be relaxed, eliminating most driving forces for aging to minimize item iv (vectoring) effects—a theme that is discussed below for TR and PIM materials.

A more flexible but stable cross-link<sup>72,73</sup> uses monoesterification of pendant carboxylic acids in 6FDA-DAM:DABA 3:2 to allow spinning and subsequent cross-linking by extending heating in the final drying step (see Figure S-1). Many diol cross-linking candidates are viable, but for the CO<sub>2</sub>/CH<sub>4</sub> pair, a propanediol cross-linked precursor with a 3:2 DAM:DABA ratio was effective.<sup>73–75</sup> Un-cross-linked PDMC (propanediol non-esterified cross-linkable) copolymer (Figure 13) dense films plasticize at 150 psia pure gas CO<sub>2</sub> feeds, but even mild sub- $T_g$  220 °C treatment extends plasticization resistance greatly (Figure 14).<sup>73</sup>

Despite adequate dense film plasticization suppression for MW < 50K samples, Omole et al.<sup>74</sup> noted that higher molecular weight polymer was needed for fiber spinning. Specifically for successful spinning and cross-linking of the dense skin, without collapse of nanoscopic transition layers (Figure 4a), a MW  $\sim$  180K was required. As with the non-ester thermal cross-link,<sup>70</sup> excess volume related to vectoring (item iv) and driving forces for aging tend to be reduced during the cross-linking. Stability in terms of both CO<sub>2</sub> permeance and CO<sub>2</sub>/CH<sub>4</sub> selectivity is

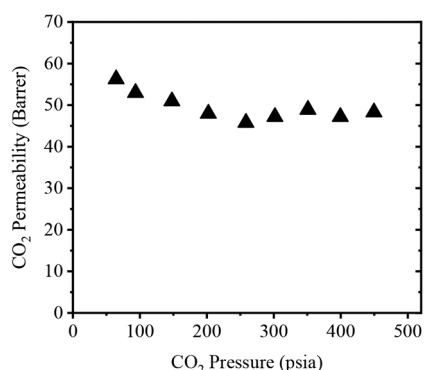


**Figure 14.** Effect of feed pressure for PDMC membranes cross-linked at 220 °C.<sup>73</sup>

shown in Figure 15 for a diverse set of binary feed compositions and pressures with 1 atm downstream permeate.<sup>74</sup>

For completeness, a short discussion of item ii (antiplasticization) is provided here, and reference to the original source<sup>75</sup> is recommended for more details. To understand the two flux depressing factors, antiplasticization (factor ii) vs Langmuir hole filling competition (factor iii), eq 3 and Figure 10 are again useful. In the absence of antiplasticization, as the excess free volume (Langmuir capacity,  $C'_{Hi}$ ) becomes saturated, permeance approaches the limit  $k_{Di}D_{Di}/L \sim 37$  GPU for CO<sub>2</sub>. Results in Figure 16 clearly fall below  $\sim 37$  GPU at high toluene ppm values, indicating that CO<sub>2</sub> diffusion coefficients are depressed by hindered formation of zones of activation for diffusive jumps.

Economical sorbent guard beds can maintain 30 ppm toluene contaminant levels for even higher contaminant levels, so in practical processes permeance and selectivity can be stable. Process upsets can occur, potentially leading to significant membrane exposure to quite high levels of condensable hydrocarbons. The effects on the cross-linked PDMC polymer in such undesirable events followed by regeneration with condensable-free conditions are shown in Figure 17. The results clearly show that temporary failure of “protective” sorbent beds are manageable. To emphasize the value of understanding antiplasticization effects for the polyimide family as approximate predictors of the other advanced TR and PIM families in Figure 6, one can consider the important study by Liu et al.<sup>76</sup> This study

considered exposure of the thermally rearranged polymer (Figure 18) HAB-6FDA TR to an essentially 50:50 CO<sub>2</sub>:CH<sub>4</sub> feed, but with up to 1700 ppm of toluene for a feed pressure of roughly 9.7 atm. As with the PDMC cross-linked polyimide fiber, large but recoverable permeability losses were seen in the HAB-6FDA TR dense film with the high toluene levels in CO<sub>2</sub>/CH<sub>4</sub>. Moreover, antiplasticization and competitive sorption effects were shown to be relevant by using the partial-immobilization dual mode model framework. Although not yet examined in asymmetric form, this study for the TR family in Figure 6 suggests similarity to the polyimide family in its ability to deliver high performance for feeds with condensable contaminants if managed properly with protective sorbent beds. Similar recoverability is anticipated for the PIM family; however, this key issue should be explored to give confidence that such fundamental issues are manageable during practical field tests.

### ■ EMPHASIZING SORPTION SELECTIVITY WHILE MAINTAINING DIFFUSION SELECTIVITY—A STILL LARGER STEP FORWARD

Many possible feeds in various venues require an additionally challenging balancing act—introducing strong sorption selectivity for one pair while maintaining good diffusion selectivity for the other pair in a ternary feed. To develop fundamentals for this balancing act, natural gas is again an ideal testbed—with practical payoffs to meet global demands.<sup>77</sup> Specifically, many “sour” natural gas reservoirs have significant H<sub>2</sub>S content as well as CO<sub>2</sub> to be stripped and reinjected rather than vented. Keeping CH<sub>4</sub> at high pressure to avoid recompression presents challenges to the polymer and membrane communities to develop and test fundamentals that can then be generalized to many other ternaries beyond natural gas feeds. Simultaneous separation of CO<sub>2</sub> and H<sub>2</sub>S from CH<sub>4</sub> is especially challenging, since the size difference between H<sub>2</sub>S (3.6 Å) and CH<sub>4</sub> (3.8 Å) pair is only 0.2 Å. To address this challenge, the more interactive nature of H<sub>2</sub>S offers a tool to adjust sorption selectivity to complement diffusion selectivity in the expression for permselectivity in eq 2. Glycol liquids, used as liquid sorbents for H<sub>2</sub>S, suggest a path to extend ester cross-linked polyimides to increase sorption selectivity for the H<sub>2</sub>S/CH<sub>4</sub> pair beyond the PDMC material in Figure 15 by using alternative cross-links.

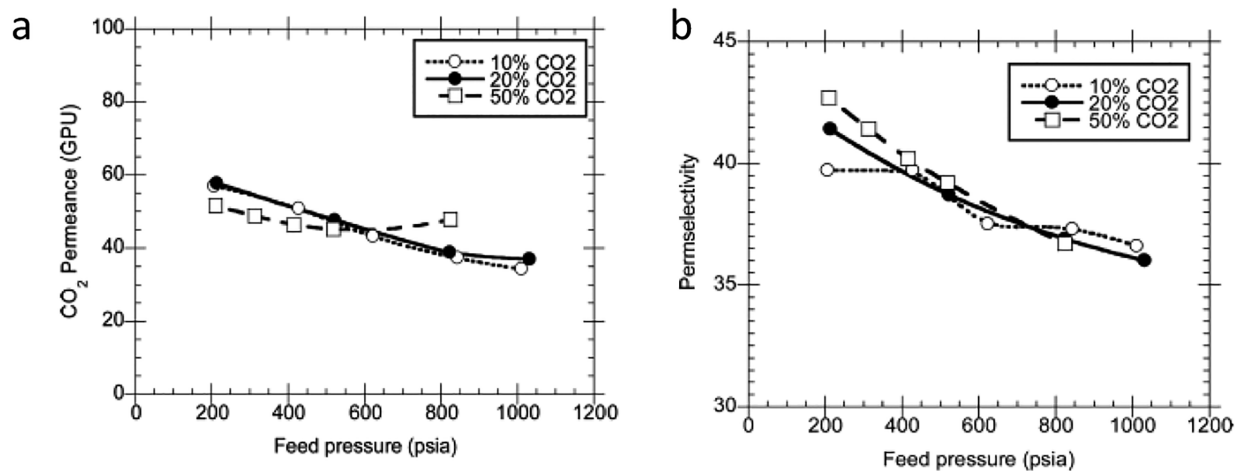


**Figure 15.** Effect of feed pressure on CO<sub>2</sub> permeance (a) and permselectivity (b) of PDMC hollow fibers cross-linked at 200 °C. Tested with an atmospheric downstream using various feed concentrations at 35 °C.<sup>74</sup>

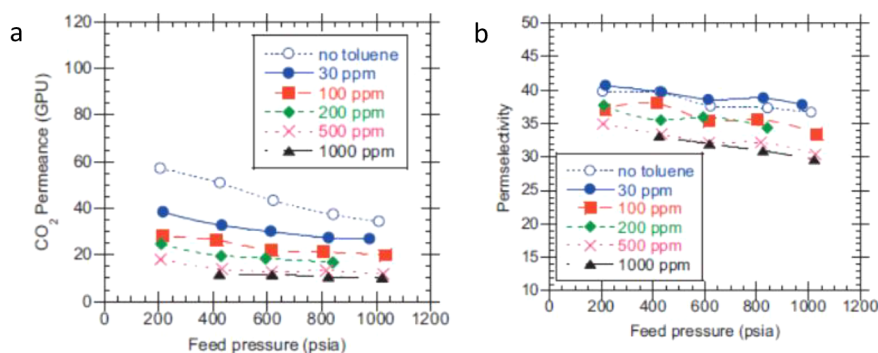


**Figure 16.** Effect of toluene at different feed pressures on the CO<sub>2</sub> permeance (a) and CO<sub>2</sub>/CH<sub>4</sub> permselectivity (b) of a cross-linked PDMC hollow fiber membrane. Tested using a 10:90 CO<sub>2</sub>:CH<sub>4</sub> mixture at 35 °C. Reproduced with permission from ref 75. Copyright 2011 Elsevier.

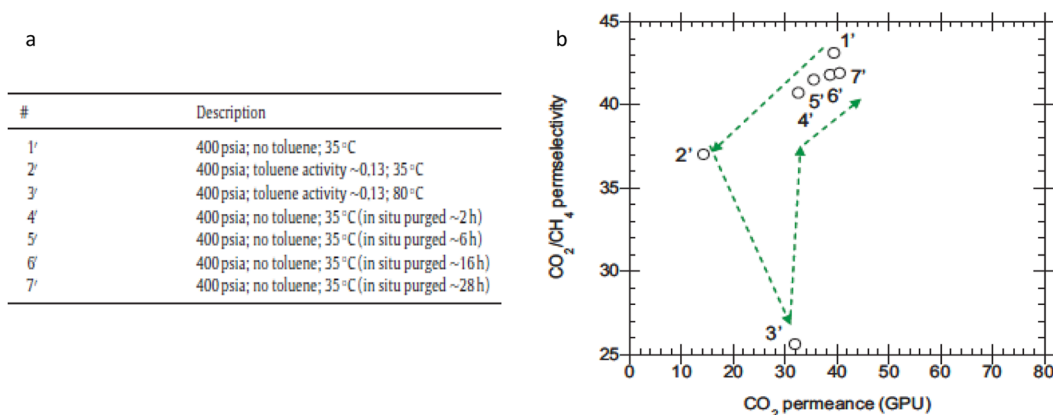


**Figure 17.** (a) Table describing test conditions fibers were exposed to. (b) Graph indicating the performance of cross-linked fibers tested under various conditions with and without impurities. The numbers beside each point indicate a test condition as described in the left table. Reproduced with permission from ref 75. Copyright Elsevier 2011.

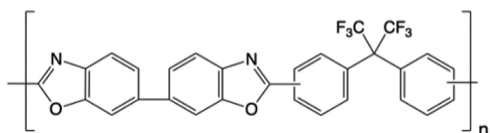


**Figure 18.** Chemical structure of HAB-6FDA TR.

Because the ternary H<sub>2</sub>S/CO<sub>2</sub>/CH<sub>4</sub> feed is more complex than the CO<sub>2</sub>/CH<sub>4</sub> pair, benchmarking any new candidate relative to PDMC with 50:50 CO<sub>2</sub>:CH<sub>4</sub> feeds is wise before confronting H<sub>2</sub>S, CO<sub>2</sub>, CH<sub>4</sub>, and contaminant containing feeds. As was done for the simpler diol cross-links leading to PDMC for CO<sub>2</sub>/CH<sub>4</sub>, dense film screening of short chain poly(ethylene glycol) (PEG) candidate cross-linkers was used as a starting point. In this regard, screening of three poly(ethylene glycol)s (diethylene glycol = DEG, triethylene glycol = TEG, tetraethylene glycol = TetraEG) were done.<sup>78</sup> All three provided acceptable cross-linked films with respective *T<sub>g</sub>*'s (374, 384, and 365 °C) vs the 385 °C *T<sub>g</sub>* for the non-esterified 6FDA:DAM-DABA 3:2.<sup>78</sup> All three PEG's suppressed H<sub>2</sub>S plasticization in dense films. The TEG cross-linkable variant (termed TEGMC) with the highest *T<sub>g</sub>* (384 °C) was expected to be best able to avoid transition layer collapse during postspinning cross-linking, so it was pursued in asymmetric format. Over 97% monoesterification of the pendant carboxyl group was achieved easily, and cross-linking at temperatures of 230, 255, and 280 °C was explored. The 255 °C cross-linking case was selected as a

good balance between economical lower temperature postspinning drying and cross-linking kinetics.<sup>79</sup>

Pure component results for dense films in Figure 19<sup>80</sup> and their fit to the dual mode model are revealing. The TEGMC, with its longer flexible TEG cross-link, compared to the simple short propanediol PDMC cross-link, shows higher CO<sub>2</sub> permeability based on the same free acid 6FDA-DAM:DABA 3:2 backbone (Figure 14 vs Figure 19). The appealing higher CO<sub>2</sub> permeability of the TEGMC shows plasticization deviation from the dual mode model for CO<sub>2</sub> above 300 psi pure CO<sub>2</sub> fugacity. On the other hand, the PDMC dense film showed no upswing in pure CO<sub>2</sub> permeability, even at 450 psia CO<sub>2</sub> for the more rigid propanediol cross-link, illustrating a trade-off between plasticization resistance and productivity. Effects of condensable contaminants like toluene are expected to show similar antiplasticization effects in TEGMC, as was seen for the PDMC case, and both cases are ideal topics for molecular simulation.

As the next logical step, the TEGMC polymer was next translated to an asymmetric format for feeds with H<sub>2</sub>S as well as CO<sub>2</sub> and CH<sub>4</sub>.<sup>79,80</sup> Possible complexities for this ternary system make it an ideal molecular simulation target. To provide actual data for such an eventual simulation study, the optimized spun and 255 °C crosslinked TEGMC was explored for CO<sub>2</sub>/CH<sub>4</sub>, H<sub>2</sub>S/CO<sub>2</sub>/CH<sub>4</sub>, and H<sub>2</sub>S/CO<sub>2</sub>/CH<sub>4</sub>/ppm toluene feeds. The high pressure 50:50 binary CO<sub>2</sub>/CH<sub>4</sub> selectivity of the cross-linked fibers (Figure 20) agreed essentially with the low pressure selectivity of 33–34 for pure component dense films, indicating

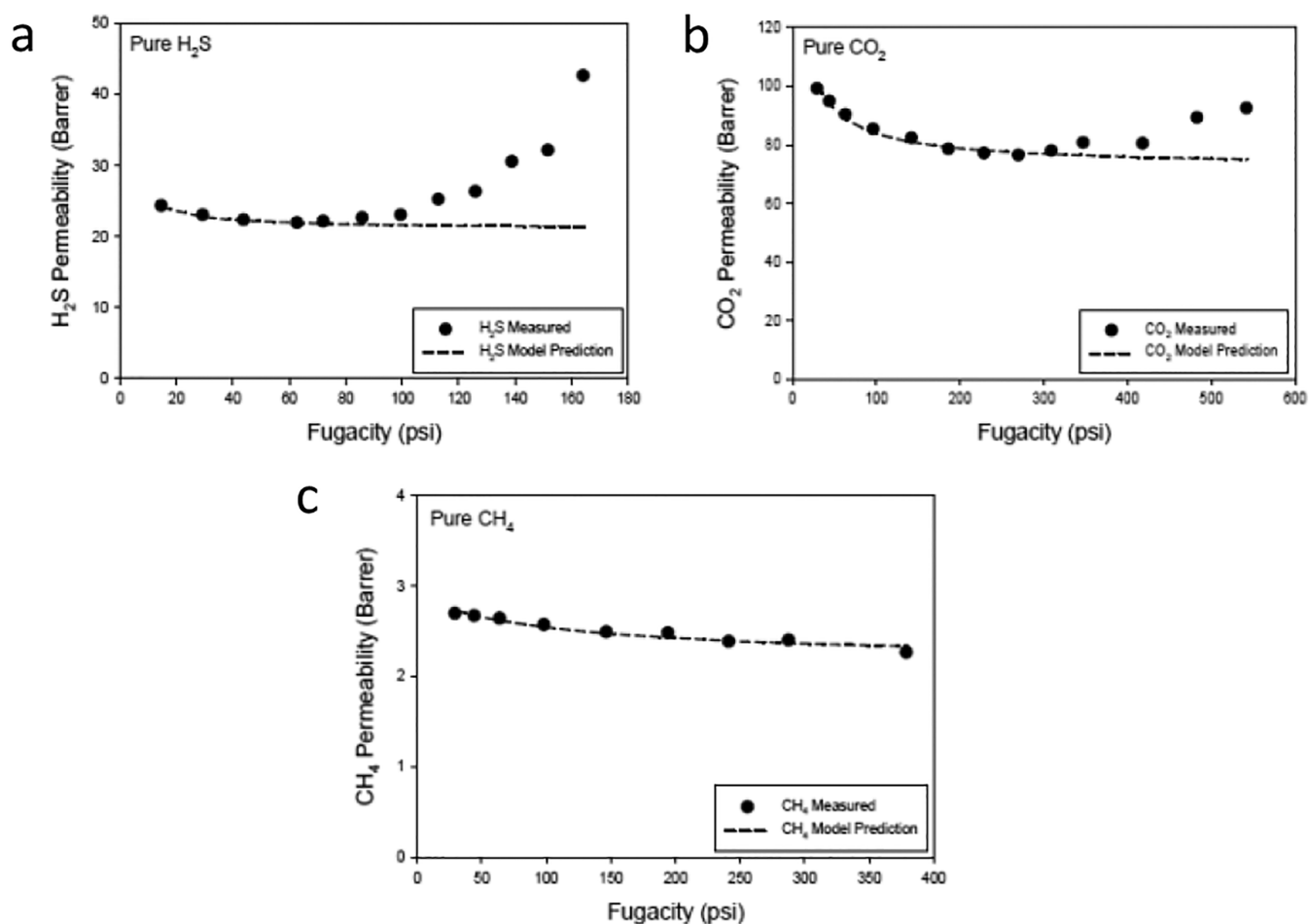


**Figure 19.** Pure gas permeation showing agreement between the experimental data and the partial immobilization model prediction at 35 °C for (a) H<sub>2</sub>S, (b) CO<sub>2</sub>, and (c) CH<sub>4</sub>. Reproduced with permission from ref 80. Copyright 2013 Kraftschik.

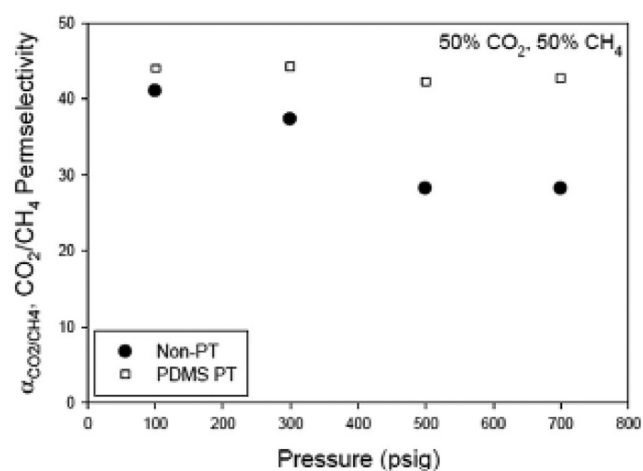


**Figure 20.** Mixed gas permeation results for cross-linked TEGMC fibers measured by using a shell-side feed with a 50:50 CO<sub>2</sub>:CH<sub>4</sub> mixture at 35 °C. Reproduced with permission from ref 79. Copyright 2018 Elsevier.

lack of defects. Nevertheless, as a useful control case, a conventional 2% PDMS (silicone rubber) post-treatment was performed, with the expectation of slightly lower permeance (due to the PDMS layer) and negligible selectivity difference for the already defect free selective layer. Binary CO<sub>2</sub>/CH<sub>4</sub> results

(Figure 20) repeatedly gave a stable selectivity of ~45 for pressures as high as 700 psia feed pressures—well above the dense film values noted above. Such post-treatments can be applied for scaled-up modules, and PDMS should be stable as a simple overcoat. In any case, as the highest performing samples the post-treated fibers are discussed next in the presence of the H<sub>2</sub>S and toluene as a desirable form of the polymer, when in asymmetric format. We speculate that the phenomenon may reflect controlled suppression of zones of activation in the presence of the thin PDMS outer layer, and while not yet well understood, it is real and reproducible. Of course, stability over months or years is required, but we believe the effect is not a traditional “leak caulking” and may be stable indefinitely. Currently, we can only say that this case provides another example of a “positive alert” about difference in asymmetric vs dense film formats and is still under study.

Results in Figure 21 for the even more challenging ternary H<sub>2</sub>S/CO<sub>2</sub>/CH<sub>4</sub> feed, which was the reason for pursuing the TEGMC, also show the attractive “positive alert” trends noted with the above binary feed. Specifically, for the ternary, CO<sub>2</sub>/CH<sub>4</sub> = 37 and H<sub>2</sub>S/CH<sub>4</sub> = 22 selectivities at 500 psia (34 atm) total pressure, again exceeding the ratio of pure component at 100 psia permeance ratios (25 for CO<sub>2</sub>/CH<sub>4</sub> and 8.8 for H<sub>2</sub>S/CH<sub>4</sub>) from Figure 19.<sup>79,80</sup> The asymptotic permeances in Figure 21 for H<sub>2</sub>S and CO<sub>2</sub> also are stable even for high pressure feeds at partial pressure (fugacities) above the onset H<sub>2</sub>S fugacity for

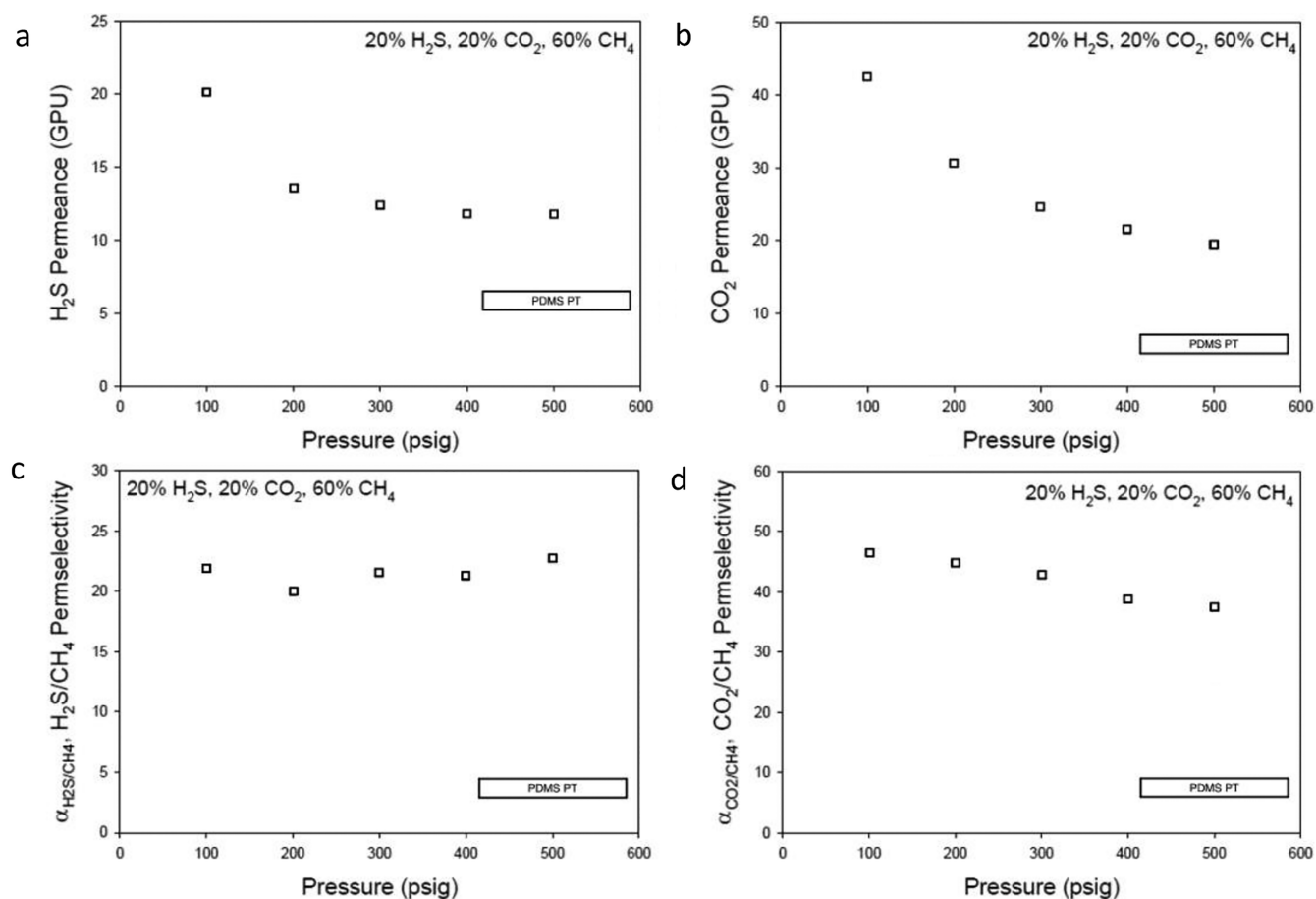


**Figure 21.** Sour gas permeance and permselectivity of cross-linked TEGMC fibers at 35 °C. H<sub>2</sub>S (a) and CO<sub>2</sub> (b) permeance isotherms and their corresponding H<sub>2</sub>S/CH<sub>4</sub> (c) and CO<sub>2</sub>/CH<sub>4</sub> (d) permselectivity isotherms are shown for a 20% H<sub>2</sub>S, 20% CO<sub>2</sub>, and 60% CH<sub>4</sub> gas mixture.

which plasticization is seen in Figure 19 for the pure component partial pressures in this complex case. Dual mode parameters for 255 °C cross-linked TEGMC fibers have not yet been measured to compare permeances to expectations from eq 3 and Figure 10.

## MINIMIZING FACTORS NEEDED FOR ADVANCED MATERIAL IMPLEMENTATION

Supplementing Figure 1 with information about (i) plasticization, (ii) antiplasticization, (iii) dual mode, and (iv) vectoring effects for new candidate materials would be welcomed by the membrane community to assist in materials selection from the ever-expanding array of available polymers. Even better would be a strategy to only require factors i–iii by removing the “vectoring” item. Reaching this goal appears possible by including results for new materials after thermal stabilization in the range of 200–300 °C for samples on low-cost uniform alumina supports.<sup>34</sup> Implementing such a plan would emphasize the practical utility of new materials that are compatible with practical processing like that in Figure S-1. The following discussion explains why this suggestion is valuable for any new polymer as illustrated by the polymer families in Figure 6.

In 1993, tetramethylhexafluoropolycarbonate (TMHFPC) (Figure 22) alerted the membrane community to what, at the time, seemed to be a drastic impact of physical aging for thin (0.4 μm) polymer layers on porous ceramic supports.<sup>34</sup> Specifically in 515 days the TMHFPC composite membrane aged from 116

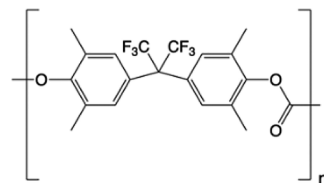


**Figure 22.** Chemical structure of TMHFPC.

to 69 barrer Helium permeability along with He/N<sub>2</sub> selectivity changes from 21 to 25.

On the other hand, thick (50–70 μm) dense film TMHFPC showed minimal changes. Typical asymmetric membranes (Figure 4 and Figure S-1) formed by conventional solvent exchange and drying show moderate permeance changes of roughly 18% over 4.5 months during ambient storage. Moreover, a cross-linkable PDMC membrane discussed in the context of avoiding CO<sub>2</sub> plasticization showed only 14% changes in CO<sub>2</sub> permeance over 8 months of ambient storage after cross-linking.<sup>81</sup> It appears that filling some fraction of the free volume in most membrane selective layers inhibits aging enough for practical storage, so once in use, aging is effectively suppressed by the permeating components. While requiring more investigation, it appears likely that the TR family, which naturally experiences elevated final thermal treatments even above those of cross-linked polyimides, will also show manageable aging for practical use. Here, therefore we focus on the PIM family in Figure 6, which is known to show stronger

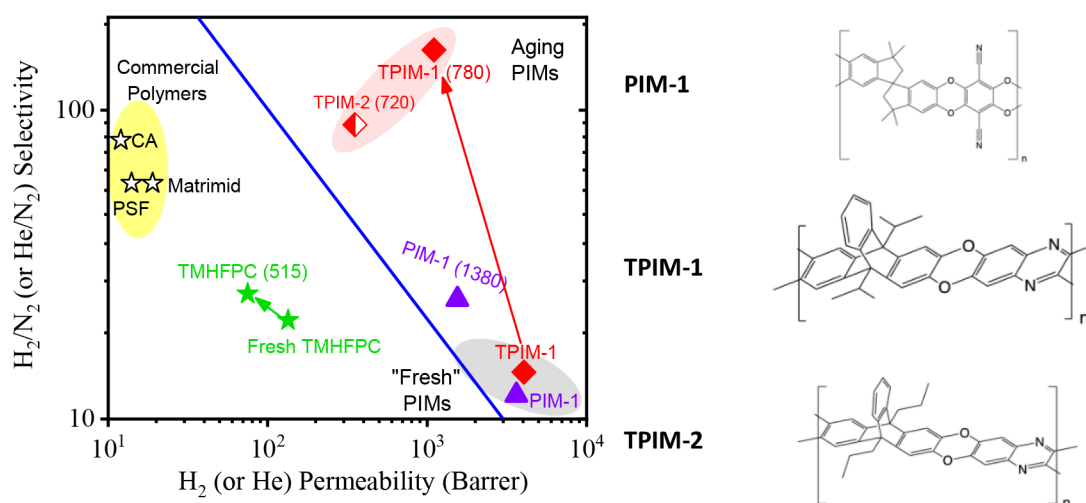


**Figure 23.** Robeson plot showing the effects of physical aging on  $\text{H}_2/\text{N}_2$  separation performance for PIMs.<sup>83</sup> The number of days aged is shown in parentheses. The solid line represents the 2008 upper bound. The chemical structures of PIM-1, TPIM-1, and TPIM-2 are also pictured to the right. A comparison between the  $\text{He}/\text{N}_2$  and  $\text{H}_2/\text{N}_2$  pair can be made. Modified from ref 83.

aging during storage. In addition, we suggest exploring a standard 200–300 °C thermal stabilization like that used for stabilized polyimides and TR polymers to suppress aging for PIMs, potentially enabling all three families in Figure 6 to be appealing for practical as well as fundamental interest.

Like the TMHFPC in Figure 22, most glassy polymers show accelerated physical aging due to more rapid free volume losses in thin vs thick layers.<sup>32–34,36,38,82–85</sup> In fact, however, even as thick (100  $\mu\text{m}$ ) dense films, the PIM family shows strong physical aging over months or years.<sup>82,85</sup> The analysis by Paul and co-workers<sup>38</sup> for standard polymers like polyimides and polycarbonates, noted earlier, is important. This analysis includes not only diffusion of free volume but also lattice contraction mechanisms<sup>86</sup> which can be at play in different specific cases. If accelerated by thermal steps like those discussed for polyimides to suppress plasticization, intrinsically high aging in PIMs, may also stabilize like other advanced polymer families useful in traditional processing (Figure S-1). If successful, this would leave only plasticization, antiplasticization, and dual mode characterization as requirements for a complete property fingerprint, which seems attractive based on the following discussion.

Figure 23 is a variant of Figure 1 for the  $\text{H}_2/\text{N}_2$  pair, which shows PIM-1 and two advanced PIMs as freshly cast thick (100  $\mu\text{m}$ ) dense films undergoing dramatic aging for 2 years in ambient storage.<sup>83</sup> On the other hand, the 0.4  $\mu\text{m}$  TMHFPC discussed earlier<sup>34</sup> in Figure 22 (taking  $\text{He}/\text{N}_2$  as a surrogate for  $\text{H}_2/\text{N}_2$ ) shows modest changes compared to the PIMs. A much smaller aging-induced selectivity change clearly occurs in the  $\text{N}_2/\text{He}$  case for the flexible TMHFPC (despite having a larger  $\Delta = 1.04$  Å size difference for  $\text{N}_2$  vs  $\text{He}$ , which should accentuate the effects of aging) as compared with  $\Delta = 0.91$  Å for  $\text{N}_2$  vs  $\text{H}_2$  for the PIM cases.<sup>83</sup> Clearly even after aging, the high permeability of the aged TPIM-1 coupled with its attractive  $\text{H}_2/\text{N}_2$  selectivity is impressive. Indeed, all three—PIM-1, TPIM-1, and TPIM-2—are more appealing than the flexible chain TMHFPC if translatable into equally thin selective layers. For PIM-1, although the aged  $\text{H}_2/\text{N}_2$  selectivity is similar to that for the TMHFPC, the PIM-1 permeability is over a factor of 10 higher than that of TMHFPC.

Size differences in A/B penetrant pairs may also help understand trends in accelerated aging for the PIM family. For example, Swaidan et al.<sup>84</sup> also did a higher temperature aging exploration, but smaller advantages were seen for the closely sized  $\text{C}_3\text{H}_6/\text{C}_3\text{H}_8$  pair with  $\Delta = 0.13$  Å between  $\text{C}_3\text{H}_6/\text{C}_3\text{H}_8$ . The smaller aging changes for the  $\text{C}_3\text{H}_6/\text{C}_3\text{H}_8$  pair compared to the case for  $\Delta = 0.91$  Å for  $\text{N}_2$  vs  $\text{H}_2$  in Figure 23 are presumably understandable in this framework. More studies of important PIMs (and other very high fractional free volume polymers) are critical to assess them more relative to the polyimides that were the focus of most discussion here. Nevertheless, connecting to practical formation process with simple final drying/annealing (Figure S-1) is also wise. Avoiding the need to track aging trajectories over months or years to assess payoff potential for key gas pairs is clearly very attractive. A modified version of Figure 2b is given in Figure 24 which may help envision effects of



**Figure 24.** Illustration of expected effects of aging in the PIM family.

free volume loss in the PIMs in Figure 24. Figure 24 seeks to convey overall tightening of the matrix, primarily by “lattice contraction”, which we considered might be the typical aging mechanism in the PIM family, as opposed to the dominant diffusion of free volume mechanism for polymers with lower and less connected fractional free volume. Such a mechanism would be consistent with very high initial penetrant diffusion through connected free volume,  $f_v$ , moderated by constrictions between quite rigid backbones. Figure 24 is, of course, also consistent with higher diffusion selectivity in the aged samples.

In any case, after casting, the characteristic initial total fractional free volume,  $f_v$ , can be evaluated from eq 5 by using the estimated occupied volume from various group contribution schemes<sup>87,88</sup> along with the as-cast specific volume,  $V_i$ .

$$f = \frac{V - V_0}{V} \quad (5)$$

We speculate that lattice contraction in PIMs is more useful to describe aging as opposed to removal of small discrete free volume packets by diffusion, responsible for most aging in more flexible backbone polyimides (Figure 22). In this regard, eq 6 from Hirai and Eyring<sup>89</sup> provides a framework, with a key material parameter,  $\tau$ , the material relaxation time, expected to have strong temperature dependence.

$$F_{LC}^* = f_g + (f_i - f_g)e^{-t/\tau} \quad (6)$$

Other forms, e.g., so-called “stretched exponential”, have also been considered,<sup>38</sup> but eq 6 is adequate for the current discussion. The hyper-rigid nature of the PIM family complicates assessment of  $f_g$ , the fractional free volume at the glass transition; however, the form of a temperature-dependent material relaxation time still applies. In fact, the rigid nature of PIMs should make material relaxation times orders of magnitude longer than the 3–5 h value at 35 °C for the polyarylate with a  $T_g$  of 195 °C studied by Paul and co-workers. If this special aging mechanism applies primarily to the PIM family, it suggests that rather than aging thick films for two years, annealing thin layers of a candidate PIM as a composite or asymmetric at 200–300 °C for several hours on a simple ceramic support may give valuable properties like those in Figure 23. Budd et al. explored annealing of PIM-1 thick films at temperatures up to 125 °C;<sup>82</sup> however, the range 200–300 °C could be more definitive along with actual analysis like that pursued for the flexible glassy polymer family.<sup>38</sup> The discussion of self-retarding behaviors illustrated by the  $O_2/N_2$  system in Figure 25 for a family of novel polyimide–

molecular-weight-related plasticization sensitivities,<sup>85</sup> which appear like those noted for the polyimide family by Mikawa et al.<sup>47</sup> Moreover, aging of higher molecular weight PIM-1 samples (100 and 230 kDa vs 60–66 kDa) show strong thickness dependent aging for 30  $\mu\text{m}$  vs 0.2  $\mu\text{m}$  dense films like those seen for traditional glassy polymers such as polyimides.<sup>85</sup> Aged high-molecular-weight thick PIM films also showed a dual mode type decreasing  $\text{CO}_2$  permeabilities response up to 8 atm, followed by plasticization up to 32 atm.<sup>84</sup> Also, decreasing  $\text{CO}_2$  permeabilities with increasing pure gas  $\text{CO}_2$  feeds up to 10 atm<sup>83</sup> and even up to 55 atm were noted<sup>91</sup> like that noted in the aged 100K and 230K molecular weight cases.<sup>85</sup> Additional work to define the critical molecular would be wise, as with the other two families in Figure 6, to clarify the molecular weight sensitivity to plasticization to avoid surprises in scaleup for plasticizing feeds. Realistically, besides experimental exploration, all three families, and still emerging families,<sup>92,93</sup> will also benefit greatly from ongoing molecular simulations to move the field forward.

## CONCLUDING COMMENTS

Glassy polymers and how (i) plasticization, (ii) antiplasticization, (iii) dual mode, and (iv) vectoring effects may be accentuated in practical asymmetric formats for high free volume for state-of-the-art membranes are important to both macromolecular and membrane communities. The materials in Figure 6 (polyimides, TR, and PIMS—and cross-family copolymer members) are viable candidates for future energy-efficient gas separations discussed here—and also larger vapor penetrants. Because of space limits, other emerging materials were not discussed, but other families will clearly eventually join the group in Figure 6. One of these families, the polybenzamidazoles,<sup>32</sup> was recently investigated by using an approach consistent with our recommendations here. Specifically, accelerating aging by sub- $T_g$  annealing at 190 °C was shown useful to stabilize permeability and selectivities for  $\text{H}_2$  vs  $\text{N}_2$  and  $\text{CH}_4$ .

The examples discussed clearly stress the need to directly address a more complete set of properties than those typically reflected in Figure 1. We noted a set of fundamental cross-cutting factors, especially if assessed in asymmetric or thin film composite forms, to guide our polymer science community in help advance gas separation membrane polymers. These factors—(i) plasticization, (ii) antiplasticization, (iii) dual mode transport, and (iv) vectoring parameters—all have fundamental roots in polymer properties. Effectively, these are “integrating factors” that provide figures of merit beyond traditionally reported features such as polymer molecular weight, glass transition temperature, and fractional free volume. If connected through molecular simulation and spectroscopy to traditionally reported properties, these factors will allow the polymer community to see better how to develop structures beyond the important, but inadequate trade-off plots such as indicated in Figure 1. Such an enriched strategy is ideally suited to gases and vapors, since the full set of properties are relatively easily assessed by modification of existing equipment and measurement procedures for key penetrants. Such an enriched strategy also sets the stage for ultimate rational movement to penetrants of larger size with relevance to additional high impact topics. For instance, recycling of unreacted paraffin in paraffin isomerization in low equilibrium conversion processes operating below 300 °C<sup>94</sup> may be possible targets. If successful, polymers in such venues can avoid the need for more costly molecular

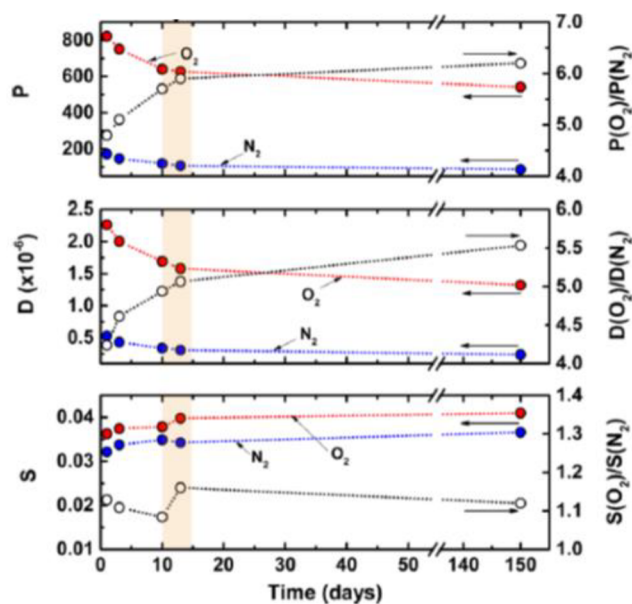


**Figure 25.** Identification of a self-retarding aging where the time dependence of gas transport properties in methanol-conditioned KAUST-PI-1 is mitigated and a quasi-steady state is reached.<sup>90</sup> Units:  $P$  [barrer] [ $10^{-10} \text{ cm}^3 \text{ (STP) cm cm}^{-2} \text{ s}^{-1} \text{ cmHg}^{-1}$ ];  $D$  [ $\text{cm}^2 \text{ s}^{-1}$ ];  $S$  [ $\text{cm}^3 \text{ (STP) cm}^{-3} \text{ cmHg}^{-1}$ ].

PIM materials further support the above suggestion for such PIM–TR copolymers as well.<sup>90</sup> In general, we expect the recommended 250–300 °C may move the most dramatic aging back to a much shorter, more attractive practical time scale of a day or so, based on the above discussion of lattice contractions. The more aggressive  $\text{CO}_2/\text{CH}_4$  pair for the PIM family reveals

sieving inorganic membranes, and they should be aspirational goals of our community.

The membrane community, by necessity, focuses on performance and cost in whatever material can deliver it attractively in a viable process like Figure S-1. By awakening to this reality, the creative polymer community will not only continue to publish interesting work but also have a practical impact in the gas separation area. Researchers on mixed matrix materials,<sup>30,93</sup> seek to understand how to leverage combinations polymer and metal–organic frameworks,<sup>95</sup> which requires attention to the types of issues we discussed here. On the other hand, carbon molecular sieve (CMS) materials rely upon rigid glassy polymers as precursors and address opportunities beyond those available to glassy polymers, such as olefin–paraffin pairs.<sup>96</sup> Selecting precursors for CMS materials is another important area for the polymer community, but like mixed matrix materials could not be discussed here due to space limitation. Nevertheless, three competitors—pure polymers, mixed matrix materials, and CMS—are united by the need to understand the topics discussed here to identify domains of opportunities for membranes to solve challenging problems. This requires attention to the integrated state-of-the-art hollow fiber formation process.<sup>97</sup>

## ■ ASSOCIATED CONTENT

### SI Supporting Information

The Supporting Information is available free of charge at <https://pubs.acs.org/doi/10.1021/acs.macromol.1c01758>.

Schematic illustration of the integrated state-of-the-art hollow fiber gas separation membrane formation process (PDF)

## ■ AUTHOR INFORMATION

### Corresponding Author

**William J. Koros** – School of Chemical & Biomolecular Engineering, Georgia Institute of Technology, Atlanta, Georgia 30332, United States; [orcid.org/0000-0001-5873-0899](https://orcid.org/0000-0001-5873-0899); Email: [wjk@chbe.gatech.edu](mailto:wjk@chbe.gatech.edu)

### Authors

**Nicholas E. León** – School of Chemical & Biomolecular Engineering, Georgia Institute of Technology, Atlanta, Georgia 30332, United States; [orcid.org/0000-0001-9411-3249](https://orcid.org/0000-0001-9411-3249)

**Zhongyun Liu** – School of Chemical & Biomolecular Engineering, Georgia Institute of Technology, Atlanta, Georgia 30332, United States

**Maryam Irani** – School of Chemical & Biomolecular Engineering, Georgia Institute of Technology, Atlanta, Georgia 30332, United States

Complete contact information is available at: <https://pubs.acs.org/10.1021/acs.macromol.1c01758>

### Notes

The authors declare no competing financial interest.

## Biographies



Nicholas León received a Bachelor of Science in Chemical and Biomolecular Engineering from the Georgia Institute of Technology in 2019. He is a chemical engineering doctoral student advised by Dr. William J. Koros at the Georgia Institute of Technology. His current research focuses on substituting energy intensive gas separation processes with more energy efficient polymer and carbon molecular sieve membranes.



Zhongyun Liu is a research engineer in the Koros Research Group in Chemical and Biomolecular Engineering at the Georgia Institute of Technology. He received his Ph.D. degree in Material Science from Tianjin University. Prior to joining the Koros Research Group, he worked as a visiting assistant researcher in the Department of Civil and Environmental Engineering at the University of California, Berkeley, from 2016 to 2018 under the guidance of Prof. Baoxia Mi. His current research interests focus on polymer membranes and carbon molecular sieve membranes for energy-efficient molecular separations.



Maryam Irani received a Ph.D. in polymer engineering from Universiti Sains Malaysia in 2014, where her dissertation focused on synthesis and characterization of hydrogel composites. She also received a Ph.D. in chemical engineering from the University of Wyoming in 2018 where she developed advanced amine-based solid sorbents for CO<sub>2</sub> capture. She has two years of postdoc experience (2019–2021) under the supervision of Professor William Koros at Georgia Institute of Technology, where her research project focused on membranes for state-of-the-art gas separations.



William Koros is the Roberto C. Goizueta Endowed Chair in Chemical and Biomolecular Engineering at the Georgia Institute of Technology. He was elected to the US National Academy of Engineering in 2000 and was named a Fellow of the American Institute of Chemical Engineers in 2002 and a Fellow of the American Association for the Advancement of Science in 2003. In 2008, Dr. Koros received the Alan S. Michaels Award for Innovation in Membrane Science and Technology from the North American Membrane Society. He received the William H. Walker Award for Excellence in Chemical Engineering Publications in 2010 and served as the 63rd Institute Lecturer for the AIChE in 2011. In 2016, Dr. Koros was selected as one of the five inaugural Fellows of the North American Membrane Society. He has 51 US patents and more than 500 refereed publications with over 30000 ISI Web of Science citations.

## ACKNOWLEDGMENTS

This work was supported by the U.S. Department of Energy Grant DE-FG02-04ER15510.

## ADDITIONAL NOTE

“Antiplasticization is used here to mean suppression of segmental motions in a polymer matrix due to the presence of low-molecular-weight additives. This differs from “suppression of plasticization” by incorporating rigid backbone moieties.

## REFERENCES

- (1) Robeson, L. M. The upper bound revisited. *J. Membr. Sci.* **2008**, *320* (1–2), 390–400.
- (2) Dal-Cin, M. M.; Kumar, A.; Layton, L. Revisiting the experimental and theoretical upper bounds of light pure gas selectivity-permeability for polymeric membranes. *J. Membr. Sci.* **2008**, *323* (2), 299–308.
- (3) Freeman, B. D. Basis of permeability/selectivity tradeoff relations in polymeric gas separation membranes. *Macromolecules* **1999**, *32* (2), 375–380.
- (4) Alentiev, A.; Yampolskii, Y. Correlation of Gas Permeability and Diffusivity with Selectivity: Orientations of the Clouds of the Data Points and the Effects of Temperature. *Ind. Eng. Chem. Res.* **2013**, *52* (26), 8864–8874.
- (5) Visser, T.; Masetto, N.; Wessling, M. Materials dependence of mixed gas plasticization behavior in asymmetric membranes. *J. Membr. Sci.* **2007**, *306* (1–2), 16–28.
- (6) Maeda, Y.; Paul, D. Effect of antiplasticization on gas sorption and transport. III. Free volume interpretation. *J. Polym. Sci., Part B: Polym. Phys.* **1987**, *25* (5), 1005–1016.
- (7) Petropoulos, J. H. On the Dual Mode Gas-Transport Model for Glassy-Polymers. *J. Polym. Sci. Pol Phys.* **1988**, *26* (5), 1009–1020.
- (8) Clausi, D. T. Formation and characterization of asymmetric polyimide hollow fiber membranes for gas separations, The University of Texas at Austin, 1998.
- (9) Koros, W. J.; Zhang, C. Materials for next-generation molecularly selective synthetic membranes. *Nat. Mater.* **2017**, *16* (3), 289–297.
- (10) Koros, W. J. Model for Sorption of Mixed Gases in Glassy-Polymers. *J. Polym. Sci. Pol Phys.* **1980**, *18* (5), 981–992.
- (11) Pfromm, P. H.; Pinnau, I.; Koros, W. J. Gas-Transport through Integral-Asymmetric Membranes - a Comparison to Isotropic Film Transport-Properties. *J. Appl. Polym. Sci.* **1993**, *48* (12), 2161–2171.
- (12) Koros, W. J.; Chern, R. T.; Stannett, V.; Hopfenberg, H. B. A Model for Permeation of Mixed Gases and Vapors in Glassy-Polymers. *J. Polym. Sci. Pol Phys.* **1981**, *19* (10), 1513–1530.
- (13) He, G. H.; Mi, Y. L.; Yue, P. L.; Chen, G. H. Theoretical study on concentration polarization in gas separation membrane processes. *J. Membr. Sci.* **1999**, *153* (2), 243–258.
- (14) Qiu, W. L.; Xu, L. R.; Chen, C. C.; Paul, D. R.; Koros, W. J. Gas separation performance of 6FDA-based polyimides with different chemical structures. *Polymer* **2013**, *54* (22), 6226–6235.
- (15) Kamaruddin, H. D.; Koros, W. J. Some observations about the application of Fick's first law for membrane separation of multi-component mixtures. *J. Membr. Sci.* **1997**, *135* (2), 147–159.
- (16) Stern, S. A. Polymers for gas separations: the next decade. *J. Membr. Sci.* **1994**, *94* (1), 1–65.
- (17) Dong, G. X.; Li, H. Y.; Chen, V. Factors affect defect-free Matrimid (R) hollow fiber gas separation performance in natural gas purification. *J. Membr. Sci.* **2010**, *353* (1–2), 17–27.
- (18) Ismail, A. F.; Yaacob, N. Performance of treated and untreated asymmetric polysulfone hollow fiber membrane in series and cascade module configurations for CO<sub>2</sub>/CH<sub>4</sub> gas separation system. *J. Membr. Sci.* **2006**, *275* (1–2), 151–165.
- (19) Shishatskiy, S.; Nistor, C.; Popa, M.; Nunes, S. P.; Peinemann, K. V. Polyimide asymmetric membranes for hydrogen separation: Influence of formation conditions on gas transport properties. *Adv. Eng. Mater.* **2006**, *8* (5), 390–397.
- (20) Kapantaidakis, G. C.; Koops, G. H.; Wessling, M.; Kaldis, S. P.; Sakellaropoulos, G. P. CO<sub>2</sub> plasticization of polyethersulfone/polyimide gas-separation membranes. *AIChE J.* **2003**, *49* (7), 1702–1711.
- (21) David, O. C.; Gorri, D.; Nijmeijer, K.; Ortiz, I.; Urtiaga, A. Hydrogen separation from multicomponent gas mixtures containing CO, N<sub>2</sub> and CO<sub>2</sub> using matrimid asymmetric hollow fiber membranes. *Procedia Engineer* **2012**, *44*, 1117–1118.
- (22) Rafiq, S.; Man, Z.; Maulud, A.; Muhammad, N.; Maitra, S. Effect of varying solvents compositions on morphology and gas permeation properties on membranes blends for CO<sub>2</sub> separation from natural gas. *J. Membr. Sci.* **2011**, *378* (1–2), 444–452.
- (23) Kim, S.; Han, S. H.; Lee, Y. M. Thermally rearranged (TR) polybenzoxazole hollow fiber membranes for CO<sub>2</sub> capture. *J. Membr. Sci.* **2012**, *403*, 169–178.
- (24) Lee, J.; Kim, J. S.; Moon, S. Y.; Park, C. Y.; Kim, J. F.; Lee, Y. M. Dimensionally-controlled densification in crosslinked thermally rearranged (XTR) hollow fiber membranes for CO<sub>2</sub> capture. *J. Membr. Sci.* **2020**, *595*, 117535.
- (25) Kim, S.; Lee, Y. M. Thermally rearranged (TR) polymer membranes with nanoengineered cavities tuned for CO<sub>2</sub> separation. *Nanotechnology for Sustainable Development* **2012**, 265–275.
- (26) Wang, Y.; Ma, X.; Ghanem, B.; Alghunaimi, F.; Pinnau, I.; Han, Y. Polymers of intrinsic microporosity for energy-intensive membrane-based gas separations. *Materials Today Nano* **2018**, *3*, 69–95.

- (27) Sánchez-Láinez, J.; Zornoza, B.; Carta, M.; Malpass-Evans, R.; McKeown, N. B.; Téllez, C.; Coronas, J. Hydrogen separation at high temperature with dense and asymmetric membranes based on PIM-EA (H<sub>2</sub>)-TB/PBI blends. *Ind. Eng. Chem. Res.* **2018**, *57* (49), 16909–16916.
- (28) Han, X.; Chen, L.; Wang, T.; Zhang, H.; Pang, J.; Jiang, Z. Ultraporous polymeric membranes based on particular ultra-rigid units for enhanced gas separation. *J. Membr. Sci.* **2021**, *629*, 119284.
- (29) Liu, J.; Xiao, Y.; Liao, K.-S.; Chung, T.-S. Highly permeable and aging resistant 3D architecture from polymers of intrinsic microporosity incorporated with beta-cyclodextrin. *J. Membr. Sci.* **2017**, *523*, 92–102.
- (30) Tamaddondar, M.; Foster, A. B.; Carta, M.; Gorgojo, P.; McKeown, N. B.; Budd, P. M. Mitigation of Physical Aging with Mixed Matrix Membranes Based on Cross-Linked PIM-1 Fillers and PIM-1. *ACS Appl. Mater. Interfaces* **2020**, *12* (41), 46756–46766.
- (31) Jue, M. L.; Breedveld, V.; Lively, R. P. Defect-free PIM-1 hollow fiber membranes. *J. Membr. Sci.* **2017**, *530*, 33–41.
- (32) Merrick, M. M.; Sujanani, R.; Freeman, B. D. Glassy polymers: Historical findings, membrane applications, and unresolved questions regarding physical aging. *Polymer* **2020**, *211*, 123176.
- (33) Struik, L. C. E. Physical aging in amorphous polymers and other materials, 1977.
- (34) Rezac, M. E.; Pfromm, P. H.; Costello, L. M.; Koros, W. J. Aging of thin polyimide-ceramic and polycarbonate-ceramic composite membranes. *Ind. Eng. Chem. Res.* **1993**, *32* (9), 1921–1926.
- (35) Victor, J. G.; Torkelson, J. M. On measuring the distribution of local free volume in glassy polymers by photochromic and fluorescence techniques. *Macromolecules* **1987**, *20* (9), 2241–2250.
- (36) Wang, H.; Chung, T.-S.; Paul, D. R. Physical aging and plasticization of thick and thin films of the thermally rearranged orthofunctional polyimide 6FDA-HAB. *J. Membr. Sci.* **2014**, *458*, 27–35.
- (37) Rowe, B. W.; Pas, S. J.; Hill, A. J.; Suzuki, R.; Freeman, B. D.; Paul, D. A variable energy positron annihilation lifetime spectroscopy study of physical aging in thin glassy polymer films. *Polymer* **2009**, *50* (25), 6149–6156.
- (38) McCaig, M.; Paul, D.; Barlow, J. Effect of film thickness on the changes in gas permeability of a glassy polyarylate due to physical aging Part II. Mathematical model. *Polymer* **2000**, *41* (2), 639–648.
- (39) McCaig, M.; Paul, D. R. Effect of film thickness on the changes in gas permeability of a glassy polyarylate due to physical aging Part I. Experimental observations. *Polymer* **2000**, *41* (2), 629–637.
- (40) Soo, C. Y.; Jo, H. J.; Lee, Y. M.; Quay, J. R.; Murphy, M. K. Effect of the chemical structure of various diamines on the gas separation of thermally rearranged poly (benzoxazole-co-imide)(TR-PBO-co-I) membranes. *J. Membr. Sci.* **2013**, *444*, 365–377.
- (41) Ye, L.; Wang, L.; Jie, X.; Yu, C.; Kang, G.; Cao, Y. Effect of hexafluoroisopropylidene group contents and treatment temperature on the performance of thermally rearranged poly (hydroxyamide) s membranes. *J. Membr. Sci.* **2020**, *595*, 117540.
- (42) Luo, S.; Zhang, Q.; Zhu, L.; Lin, H.; Kazanowska, B. A.; Doherty, C. M.; Hill, A. J.; Gao, P.; Guo, R. Highly selective and permeable microporous polymer membranes for hydrogen purification and CO<sub>2</sub> removal from natural gas. *Chem. Mater.* **2018**, *30* (15), 5322–5332.
- (43) Hoehn, H. Heat treatment of membranes of selected polyimides, polyesters and polyamides, 1974.
- (44) Pye, D.; Hoehn, H.; Panar, M. Measurement of gas permeability of polymers. II. Apparatus for determination of permeabilities of mixed gases and vapors. *J. Appl. Polym. Sci.* **1976**, *20* (2), 287–301.
- (45) Pye, D.; Hoehn, H.; Panar, M. Measurement of gas permeability of polymers. I. Permeabilities in constant volume/variable pressure apparatus. *J. Appl. Polym. Sci.* **1976**, *20* (7), 1921–1931.
- (46) Coleman, M.; Koros, W. Conditioning of fluorine containing polyimides. 1. Effect of exposure to high pressure carbon dioxide on permeability. *Macromolecules* **1997**, *30* (22), 6899–6905.
- (47) Mikawa, M.; Nagaoka, S.; Kawakami, H. Gas permeation stability of asymmetric polyimide membrane with thin skin layer: effect of molecular weight of polyimide. *J. Membr. Sci.* **2002**, *208* (1–2), 405–414.
- (48) Neyertz, S.; Brown, D. Single-and mixed-gas sorption in large-scale molecular models of glassy bulk polymers. Competitive sorption of a binary CH<sub>4</sub>/N<sub>2</sub> and a ternary CH<sub>4</sub>/N<sub>2</sub>/CO<sub>2</sub> mixture in a polyimide membrane. *J. Membr. Sci.* **2020**, *614*, 118478.
- (49) Kim, T.H.; Koros, W.J.; Husk, G.R.; O'Brien, K.C. Relationship between Gas Separation Properties and Chemical-Structure in a Series of Aromatic Polyimides. *J. Membr. Sci.* **1988**, *37* (1), 45–62.
- (50) Matsumoto, K.; Xu, P. Gas Permeation Properties of Hexafluoro Aromatic Polyimides. *J. Appl. Polym. Sci.* **1993**, *47* (11), 1961–1972.
- (51) Hayes, R. A. Polyimide gas separation membranes. US4717393, 1988.
- (52) Hayes, R. A. Polyimide gas separation membranes. US4705540, 1987.
- (53) Hayes, R. A. Polyimide gas separation membranes. US4717394, 1988.
- (54) Hayes, R. A. Polyimide gas separation membranes. US4838900, 1989.
- (55) Chern, R. T.; Koros, W. J.; Hopfenberg, H. B.; Stannett, V. T. Reversible Isopentane-Induced Depression of Carbon-Dioxide Permeation through Polycarbonate. *J. Polym. Sci. Pol Phys.* **1983**, *21* (5), 753–763.
- (56) Ruiz-Treviño, F.; Paul, D. Modification of polysulfone gas separation membranes by additives. *J. Appl. Polym. Sci.* **1997**, *66* (10), 1925–1941.
- (57) Wu, S. S.; Liang, J. C.; Shi, Y. P.; Huang, M. H.; Bi, X. Y.; Wang, Z. G.; Jin, J. Design of interchain hydrogen bond in polyimide membrane for improved gas selectivity and membrane stability. *J. Membr. Sci.* **2021**, *618*, 118659.
- (58) Gleason, K. L.; Smith, Z. P.; Liu, Q.; Paul, D. R.; Freeman, B. D. Pure- and mixed-gas permeation of CO<sub>2</sub> and CH<sub>4</sub> in thermally rearranged polymers based on 3,3'-dihydroxy-4,4'-diamino-biphenyl (HAB) and 2,2'-bis-(3,4-dicarboxyphenyl) hexafluoropropane dianhydride (6FDA). *J. Membr. Sci.* **2015**, *475*, 204–214.
- (59) Li, P.; Chung, T. S.; Paul, D. R. Temperature dependence of gas sorption and permeation in PIM-1. *J. Membr. Sci.* **2014**, *450*, 380–388.
- (60) Kim, S. J.; Jo, H. J.; Lee, Y. M. Sorption and transport of small gas molecules in thermally rearranged (TR) polybenzoxazole membranes based on 2,2-bis(3-amino-4-hydroxyphenyl)-hexafluoropropane (bis-APAF) and 4,4'-hexafluoroisopropylidene diphthalic anhydride (6FDA). *J. Membr. Sci.* **2013**, *441*, 1–8.
- (61) Carta, M.; Bernardo, P.; Clarizia, G.; Jansen, J. C.; McKeown, N. B. Gas Permeability of Hexaphenylbenzene Based Polymers of Intrinsic Microporosity. *Macromolecules* **2014**, *47* (23), 8320–8327.
- (62) Visser, T.; Koops, G. H.; Wessling, M. On the subtle balance between competitive sorption and plasticization effects in asymmetric hollow fiber gas separation membranes. *J. Membr. Sci.* **2005**, *252* (1–2), 265–277.
- (63) Bos, A.; Punt, I.; Strathmann, H.; Wessling, M. Suppression of gas separation membrane plasticization by homogeneous polymer blending. *AIChE J.* **2001**, *47* (5), 1088–1093.
- (64) Barsema, J. N.; Kapantaidakis, G. C.; van der Vegt, N. F. A.; Koops, G. H.; Wessling, M. Preparation and characterization of highly selective dense and hollow fiber asymmetric membranes based on BTDA-TDI/MDI co-polyimide. *J. Membr. Sci.* **2003**, *216* (1–2), 195–205.
- (65) Cao, C.; Wang, R.; Chung, T. S.; Liu, Y. Formation of high-performance 6FDA-2,6-DAT asymmetric composite hollow fiber membranes for CO<sub>2</sub>/CH<sub>4</sub> separation. *J. Membr. Sci.* **2002**, *209* (1), 309–319.
- (66) Cao, C.; Chung, T. S.; Liu, Y.; Wang, R.; Pramoda, K. P. Chemical cross-linking modification of 6FDA-2,6-DAT hollow fiber membranes for natural gas separation. *J. Membr. Sci.* **2003**, *216* (1–2), 257–268.
- (67) Chung, T.-S.; Ren, J.; Wang, R.; Li, D.; Liu, Y.; Pramoda, K.; Cao, C.; Loh, W. W. Development of asymmetric 6FDA-2, 6DAT hollow fiber membranes for CO<sub>2</sub>/CH<sub>4</sub> separation: Part 2. Suppression of plasticization. *J. Membr. Sci.* **2003**, *214* (1), 57–69.

- (68) Zhang, C. L.; Cao, B.; Li, P. Thermal oxidative crosslinking of phenolphthalein-based cardo polyimides with enhanced gas permeability and selectivity. *J. Membr. Sci.* **2018**, *546*, 90–99.
- (69) Kratochvil, A. M.; Koros, W. J. Decarboxylation-Induced Cross-Linking of a Polyimide for Enhanced CO<sub>2</sub> Plasticization Resistance. *Macromolecules* **2008**, *41* (21), 7920–7927.
- (70) Qiu, W. L.; Chen, C. C.; Xu, L. R.; Cui, L. L.; Paul, D. R.; Koros, W. J. Sub-T-g Cross-Linking of a Polyimide Membrane for Enhanced CO<sub>2</sub> Plasticization Resistance for Natural Gas Separation. *Macromolecules* **2011**, *44* (15), 6046–6056.
- (71) Chen, C. C.; Miller, S. J.; Koros, W. J. Characterization of Thermally Cross-Linkable Hollow Fiber Membranes for Natural Gas Separation. *Ind. Eng. Chem. Res.* **2013**, *52* (3), 1015–1022.
- (72) Wind, J. D. Improving polyimide membrane resistance to carbon dioxide plasticization in natural gas separations, The University of Texas at Austin, 2002.
- (73) Hillock, A. M. W.; Koros, W. J. Cross-linkable polyimide membrane for natural gas purification and carbon dioxide plasticization reduction. *Macromolecules* **2007**, *40* (3), 583–587.
- (74) Omole, I. C.; Adams, R. T.; Miller, S. J.; Koros, W. J. Effects of CO<sub>2</sub> on a High Performance Hollow-Fiber Membrane for Natural Gas Purification. *Ind. Eng. Chem. Res.* **2010**, *49* (10), 4887–4896.
- (75) Omole, I. C.; Bhandari, D. A.; Miller, S. J.; Koros, W. J. Toluene impurity effects on CO<sub>2</sub> separation using a hollow fiber membrane for natural gas. *J. Membr. Sci.* **2011**, *369* (1–2), 490–498.
- (76) Liu, Q.; Galizia, M.; Gleason, K. L.; Scholes, C. A.; Paul, D. R.; Freeman, B. D. Influence of toluene on CO<sub>2</sub> and CH<sub>4</sub> gas transport properties in thermally rearranged (TR) polymers based on 3,3'-dihydroxy-4,4'-diamino-biphenyl (HAB) and 2,2'-bis-(3,4-dicarboxyphenyl) hexafluoropropane dianhydride (6FDA). *J. Membr. Sci.* **2016**, *514*, 282–293.
- (77) Mazyan, W.; Ahmadi, A.; Ahmed, H.; Hoorfar, M. Market and technology assessment of natural gas processing: A review. *J. Nat. Gas Sci. Eng.* **2016**, *30*, 487–514.
- (78) Kraftschik, B.; Koros, W. J. Cross-Linkable Polyimide Membranes for Improved Plasticization Resistance and Permselectivity in Sour Gas Separations. *Macromolecules* **2013**, *46* (17), 6908–6921.
- (79) Babu, V. P.; Kraftschik, B. E.; Koros, W. J. Crosslinkable TEGMC asymmetric hollow fiber membranes for aggressive sour gas separations. *J. Membr. Sci.* **2018**, *558*, 94–105.
- (80) Kraftschik, B. E. Advanced crosslinkable polyimide membranes for aggressive sour gas separations, Georgia Institute of Technology, 2013.
- (81) Liu, G.; Li, N.; Miller, S. J.; Kim, D.; Yi, S.; Labreche, Y.; Koros, W. J. Molecularly Designed Stabilized Asymmetric Hollow Fiber Membranes for Aggressive Natural Gas Separation. *Angew. Chem., Int. Ed. Engl.* **2016**, *55* (44), 13754–13758.
- (82) Bernardo, P.; Bazzarelli, F.; Tasselli, F.; Clarizia, G.; Mason, C. R.; Maynard-Atem, L.; Budd, P. M.; Lanc, M.; Pilnacek, K.; Vopicka, O.; Friess, K.; Fritsch, D.; Yampolskii, Y. P.; Shantarovich, V.; Jansen, J. C. Effect of physical aging on the gas transport and sorption in PIM-1 membranes. *Polymer* **2017**, *113*, 283–294.
- (83) Swaidan, R.; Ghanem, B.; Litwiller, E.; Pinnau, I. Physical Aging, Plasticization and Their Effects on Gas Permeation in “Rigid” Polymers of Intrinsic Microporosity. *Macromolecules* **2015**, *48* (18), 6553–6561.
- (84) Swaidan, R. J.; Ma, X. H.; Litwiller, E.; Pinnau, I. Enhanced propylene/propane separation by thermal annealing of an intrinsically microporous hydroxyl-functionalized polyimide membrane. *J. Membr. Sci.* **2015**, *495*, 235–241.
- (85) Tiwari, R. R.; Jin, J. Y.; Freeman, B. D.; Paul, D. R. Physical aging, CO<sub>2</sub> sorption and plasticization in thin films of polymer with intrinsic microporosity (PIM-1). *J. Membr. Sci.* **2017**, *537*, 362–371.
- (86) Curro, J. G.; Lagasse, R. R.; Simha, R. Diffusion-Model for Volume Recovery in Glasses. *Macromolecules* **1982**, *15* (6), 1621–1626.
- (87) Van Krevelen, D. *Properties of Polymers*, 3rd ed.; Elsevier Science: New York, 1990.
- (88) Park, J. Y.; Paul, D. R. Correlation and prediction of gas permeability in glassy polymer membrane materials via a modified free volume based group contribution method. *J. Membr. Sci.* **1997**, *125* (1), 23–39.
- (89) Hirai, N.; Eyring, H. Bulk Viscosity of Polymeric Systems. *J. Polym. Sci.* **1959**, *37* (131), 51–70.
- (90) Swaidan, R.; Al-Saeedi, M.; Ghanem, B.; Litwiller, E.; Pinnau, I. Rational Design of Intrinsically Ultramicroporous Polyimides Containing Bridgehead-Substituted Triptycene for Highly Selective and Permeable Gas Separation Membranes. *Macromolecules* **2014**, *47* (15), 5104–5114.
- (91) Du, N. Y.; Dal-Cin, M. M.; Robertson, G. P.; Guiver, M. D. Decarboxylation-Induced Cross-Linking of Polymers of Intrinsic Microporosity (PIMs) for Membrane Gas Separation. *Macromolecules* **2012**, *45* (12), 5134–5139.
- (92) Corrado, T.; Guo, R. L. Macromolecular design strategies toward tailoring free volume in glassy polymers for high performance gas separation membranes. *Mol. Syst. Des. Eng.* **2020**, *5* (1), 22–48.
- (93) Galizia, M.; Chi, W. S.; Smith, Z. P.; Merkel, T. C.; Baker, R. W.; Freeman, B. D. 50th Anniversary Perspective: Polymers and Mixed Matrix Membranes for Gas and Vapor Separation: A Review and Prospective Opportunities. *Macromolecules* **2017**, *50* (20), 7809–7843.
- (94) Sullivan, D.; Metro, S.; Pujado, P. R. *Isomerization in Petroleum Processing*; Springer International Publishing: 2015; pp 479–497.
- (95) Bachman, J. E.; Smith, Z. P.; Li, T.; Xu, T.; Long, J. R. Enhanced ethylene separation and plasticization resistance in polymer membranes incorporating metal-organic framework nanocrystals. *Nat. Mater.* **2016**, *15* (8), 845–9.
- (96) Salleh, W. N. W.; Ismail, A. F.; Matsuura, T.; Abdullah, M. S. Precursor Selection and Process Conditions in the Preparation of Carbon Membrane for Gas Separation: A Review. *Sep Purif Rev.* **2011**, *40* (4), 261–311.
- (97) Carruthers, S. B.; Ramos, G. L.; Koros, W. J. Morphology of integral-skin layers in hollow-fiber gas-separation membranes. *J. Appl. Polym. Sci.* **2003**, *90*, 399–411.

## Recommended by ACS

### Molecular Order Determines Gas Transport through Smectic Liquid Crystalline Polymer Membranes with Different Chemical Compositions

Joey Kloos, Zandrie Bormeman, *et al.*

SEPTEMBER 22, 2022  
ACS APPLIED POLYMER MATERIALS

READ 

### Compatibility of High-Density Polyethylene Piping and Associated Elastomers with the Renewable Fuels Ammonia and Dimethyl Ether

Yuecheng Zhang, Colin A. Scholes, *et al.*

NOVEMBER 17, 2022  
ENERGY & FUELS

READ 

### Scalable Pillar[5]arene-Integrated Poly(arylate-amide) Molecular Sieve Membranes to Separate Light Gases

Woochul Song, Manish Kumar, *et al.*

JULY 15, 2022  
CHEMISTRY OF MATERIALS

READ 

### Spirobisindane-Containing Imidazolium Polyimide Ionene: Structural Design and Gas Separation Performance of “Ionic PIMs”

Irshad Kammakam, Enrique M. Jackson, *et al.*

MAY 31, 2022  
MACROMOLECULES

READ 

Get More Suggestions >